This article has been accepted for publication in IEEE Transactions on Intelligent Vehicles. This is the author's version which has not been fully edited and content may change prior to final publication. Citation information: DOI 10.1109/TIV.2024.3404658

A Lane-Changing Trajectory Planning Algorithm Based on Lane-Change Impact Prediction

Xiaoxia Xiong, Yu He, Yingfeng Cai, Qingchao Liu, Hai Wang, Long Chen

***Abstract*—Current research on lane-changing trajectory planning typically focuses on the benefits of the Subject Vehicle (SV), including factors such as lane-changing efficiency, comfort, and safety. However, this can result in disturbances to the normal driving of the following vehicles. To address this issue, this paper proposes a lane-changing trajectory planning algorithm that takes into account the impact of lane changes. Based on the trajectories of the following vehicles, a gap distance-based evaluation scheme is first proposed to judge whether a vehicle is affected by the lane change of SV. An ordered probit model is then developed to predict the number of vehicles affected, with their efficiency and comfort benefits incorporated into the cost function for SV's lane-changing trajectory planning. Safety evaluation of the planned trajectories is further performed using an improved predictive risk field that can comprehensively quantify the risk posed by the surrounding vehicles. Finally, verification is conducted using the Simulation of Urban Mobility (SUMO) platform, and the results show that the proposed algorithm generates optimal lane-changing trajectories that maximize the overall benefits for multiple relevant vehicles when compared with other existing algorithms.**

Keywords*—*Lane-changing impacts, Connected autonomous vehicles, Lane-changing trajectory planning, Multi-vehicle benefits, Risk potential field

I. Introduction

UNSAFE lane-changing maneuvers cause approximately 5% of traffic accidents in the United States each year [1]. Additionally, poor lane-changing behavior can trigger the formation and propagation of stop-and-go shock waves and lead to traffic congestion [2]. As a result, how to plan safe and efficient lane-changing trajectories is a crucial research topic for the development of Connected Autonomous Vehicles (CAVs). Previous research on lane-changing trajectory planning mainly considers the benefits to the Subject Vehicle (SV), such as its lane change efficiency, comfort, and safety. However, such prioritization on SV may affect the normal driving of vehicles behind it. While some research has delved into cooperative control strategies for fleets to enhance overall driving efficiency [3], limited attention has been paid to mitigating traffic flow fluctuations by controlling lane-changing vehicles, which can be particularly relevant in the current context as human drivers still dominate road traffic. In [4] and [5], new lane-changing decision-making strategies were developed to reduce the negative impact of irrational lane-change decisions on traffic flow, but the details of lane-changing trajectories were not considered. Li et al. [6] proposed a lane-changing trajectory algorithm to optimize the overall benefits of SV and its following vehicles. However, they simply took the 10 vehicles behind SV in the target lane as affected vehicles in cost function evaluation. There remains a gap in determining which surrounding vehicles will be affected by the lane-changing behavior and should be included in the research scope of lane-changing trajectory planning. If the range is too large, excessive computing power will be wasted, and the study will become more complicated. Conversely, if the range is too small, the trajectory planning results may have a greater impact on the surrounding normal vehicles due to insufficient consideration.

Many studies have researched the impact of lane change on traffic flow from different perspectives [7]-[12]. Zheng et al. [9] analyzed the effect of lane change on the formation and development of traffic oscillations based on trajectory data. Li et al. [10] described the impact of lane change using the difference between the average flow volume in the front and behind the lane-changing vehicle, and trained a Support Vector Regression (SVR) model to predict it. He et al. [11] proposed a method to capture the spatial-temporal impact of lane change on the surrounding traffic through the decreasing and increasing law of minimum space. Yang et al. [12] developed sinusoidal and DossRsep models to simulate the speed change of the first following vehicle on the target lane during the lane-changing process of SV, and further found out the overall delay of the fleet. However, there is still a lack of specific mathematical formulas applicable to determining how many surrounding vehicles are affected by the lane-changing vehicle.

Safety evaluation also plays a critical part in lane-changing trajectory planning, as lane-changing typically involves multi-vehicle interactions and risk stacking [13]. Existing research on trajectory planning typically screens trajectories based on collision and kinematic constraints to ensure lane-changing safety [14],[15]. To achieve better planning outcomes, the risk level of the candidate trajectories that already meet the basic constraints should be further evaluated and distinguished using risk assessment methods [16]. In [17], common risk thresholds derived from the NGSIM and highD datasets were utilized to classify planning trajectories into low, medium, or high-risk categories. Wu et al. [18] developed a spatial-temporal risk identification model for lane change based on fault tree analysis, which is capable of capturing the interaction risk among the trajectories of SV and its

This work is supported by the National Natural Science Foundation of China (52225212, 52372413, 52072160, U20A20331), National Key R&D Program of China (2023YFB2504403), and Graduate Research & Practice Innovation Program of Jiangsu Province (No. KYCX23_3670).

The authors are with School of Automotive and Traffic Engineering, Jiangsu University, Zhenjiang, Jiangsu, China. (Corresponding author: lqc@ujs.edu.cn).

This article has been accepted for publication in IEEE Transactions on Intelligent Vehicles. This is the author's version which has not been fully edited and content may change prior to final publication. Citation information: DOI 10.1109/TIV.2024.3404658

surrounding vehicles. Cai et al. [19] proposed a complex network-based vehicle risk cognitive system using a variable Gaussian safety field, which is suitable for evaluating the multi-vehicle risks associated with lane changes. Lee et al. [20] used a predictive occupancy map to calculate the potential risk associated with surrounding vehicles and assess the risk level of collision avoidance trajectories. Most of these studies have not considered the potential impact of varying acceleration of the interacting vehicles probably due to the difficulty in obtaining accurate acceleration data. However, in the Internet of Vehicles (IoV) environment, obtaining accurate acceleration is no longer a difficult task.

In summary, current research has two main shortcomings. Firstly, there is a lack of lane-changing trajectory planning algorithms that can consider the common interests of SV and surrounding affected vehicles by determining the influence range of lane change. Secondly, the trajectory risk evaluation in lane-changing trajectory planning often ignores the variation in acceleration. Aiming at these problems, this paper makes a two-fold contribution:

(1) a novel lane-changing influence range evaluation scheme is proposed and a prediction model is established for lane-changing trajectory planning of CAVs to reduce their impact on the rear traffic flow;

(2) an improved predictive risk field model accounting for varying acceleration is established to quantify the interaction risk between SV and its surrounding vehicles.

The overall framework of this paper is shown in Fig. 1.

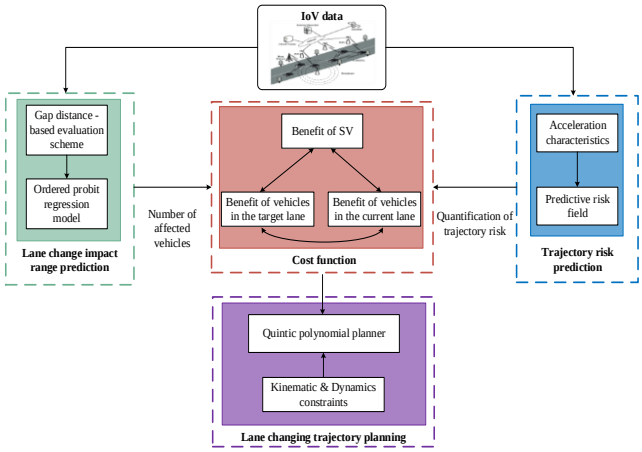

Fig. 1. Overall framework of the paper

The rest of the paper is structured as follows. In section II, the relevant literature on trajectory planning will be discussed. A lane-changing impact evaluation scheme and prediction model will be introduced in section III. Section IV presents the trajectory planning algorithm considering the affected vehicles. The results and conclusions will be discussed in section V and section VI.

II. LITERATURE REVIEW

In this section, the typical algorithms of trajectory planning are reviewed, and the research gap for the proposed framework is identified.

The task of trajectory planning is to calculate a collision-free trajectory that enables the vehicle to travel from its initial position to its destination based on the planned motion behavior determined at the decision-making level. The destination can vary based on situation-specific local objectives [21], e.g., it may be a few meters ahead of the current lane, of the left lane, or in front of the stop line at the next intersection. There are two main trajectory planning methods: the direct construction method and the path-velocity decomposition method. The direct construction method simultaneously generates path and velocity curves, typically using curve interpolation or the MPC algorithm. In contrast, the path-velocity decomposition method first constructs a spatial path from the start point to the end point and then performs velocity planning based on the path. Specifically, trajectory planning algorithms can be classified into the following five categories based on their calculation characteristics.

(1) Graph search-based algorithm: the optimal path is found on the constructed grid graph using algorithms such as Dijkstra and A*. Stahl et al. [22] generated a series of state lattices in the natural coordinate system and connected them with spline curves to compute the lowest cost trajectory by the graph search method. The real-time trajectory planning algorithm was validated through simulation and real vehicle testing. Tanzmeister et al. [23] allowed edges in the state grid to be at any continuous position within a discrete cell, and combined the A* algorithm with Rapidly-exploring Random Trees (RRT) to search for optimal paths for lane keeping and changing maneuvers (left-turn, right-turn). The graph search-based method usually involves complex environmental modeling and has low computational efficiency, making it more suitable for global path planning.

(2) Sampling-based algorithm: random or regular sampling points are generated in the traveling space and are connected according to certain conditions. The resulting sequence of sampling points that meet the conditions forms the generated path. Typical algorithms include RRT and Probabilistic Road Maps (PRM). Such sampling method is probabilistically complete but cannot guarantee driving comfort, and thus further curve smoothing and angle smoothing are necessary. Guy et al. [24] utilized a sampling algorithm to generate feasible clusters of trajectories by combining behavioral and motion planning, and obtained the optimal decisions and trajectories that minimize the cost function. Similarly, Shen et al. [25] constructed a cost graph describing the risk of vehicle interaction and planned the optimal paths by the RRT* algorithm.

(3) Curve interpolation-based algorithm: path or velocity curves are generated using a preset form of curve, such as polynomial curves, Bézier curves, and spline curves. This method focuses on the smooth connection between coordinate points rather than the actual planning task, and is usually used in conjunction with other trajectory planning methods. However, in more refined scenarios, such as lane-changing scenarios, the curve interpolation method is adequate as a standalone planning method. Yang et al. [26] used a multidimensional time-series regression approach to calibrate the personalized parameters for longitudinal and lateral trajectories with real driving data, and established a

This article has been accepted for publication in IEEE Transactions on Intelligent Vehicles. This is the author's version which has not been fully edited and content may change prior to final publication. Citation information: DOI 10.1109/TIV.2024.3404658

set of hyperbolic orthogonal lane-changing trajectories that can accommodate different driver styles. Chen et al. [27] proposed a lane-changing trajectory planning method for collision avoidance using a three-dimensional Bessel curve. Specifically, two asymmetric third-order Bessel curves were used to plan the collision avoidance and lane-changing paths respectively, and the speed planning of the two paths was performed on the z-axis. The simulation results demonstrated that the segmented Bezier curve lane-changing trajectory can be adapted to different scenarios and improve the safety of the lane-changing process.

(4) Numerical optimization-based algorithm: trajectory planning is described as a mathematical problem of finding the minimum or maximum value of an objective function within a variety of constraints. The optimization objectives typically include driving safety, stability, comfort, and efficiency. The constraints that need to be considered include vehicle acceleration/ deceleration, non-integrity, and kinematic and dynamic constraints. Zhang et al. [28] solved a coarse-grained trajectory using a static risk cooperative game of path and velocity, and then used quadratic programming to obtain a fine-grained smooth trajectory. Lim et al. [29] proposed a hybrid trajectory planning approach to integrate the advantages of sampling and numerical optimization methods.

(5) Artificial potential field-based algorithm: a gravitational field and a repulsive field are set up for the target point and the obstacle, respectively, and optimization methods such as gradient descent are used to solve for the optimal path under the effect of the potential field. The method is intuitive and easy to understand, but it may lead to a locally optimal solution. To overcome this issue, Ji et al. [30] proposed a three-dimensional potential field that combines an elliptic potential field with a Gaussian velocity field. The results showed that the planner based on this mixed field can avoid the local minimum problem of the traditional potential field. Xie et al. [31] proposed a distributed motion planning approach based on an improved artificial potential field, which enables the autonomous vehicle to complete overtaking of a dynamic human-controlled vehicle.

Existing studies on lane-changing trajectory planning have different focuses and expect to design various types of trajectory profiles to solve the problems of complex scenarios[32],[33], emissions[34], efficiency[35], safety[36], and personalization[37]. However, these studies have neglected the interests of surrounding vehicles, i.e., although SV can perform efficient lane changes, it may negatively affect the following vehicles, which may generate traffic shockwaves or even cause traffic accidents. In other words, CAVs should take social responsibility when changing lanes to avoid disrupting the normal movement of surrounding vehicles, thus promoting the overall benefits of the transport system. Taking these into account, we propose a lane-changing trajectory planning algorithm that integrates the benefits of SV and surrounding vehicles using a numerical optimization-based framework, which will be presented in detail in Sections III and IV.

III. Prediction Method for the Impact Range of Lane Changing

In this section, a gap distance-based evaluation scheme is first proposed to determine if a given vehicle is affected by lane changing, and then an ordered probit model is established to predict the extent to which the lane changing behavior affects the traffic behind.

A. Gap distance-based evaluation scheme

Inspired by [11], this study proposes a gap distance-based evaluation scheme to determine whether the surrounding vehicles are affected by the lane changing of SV. The variation in gap distance between vehicles resulting from the lane change of SV can be analyzed from the perspectives of the current and target lanes of SV, respectively:

- Current lane: when SV changes lane, the reachable space of the rear vehicle immediately behind it in the current lane (represented as R1) changes, as the front vehicle of R1 changes from SV to the initial preceding vehicle of SV in the current lane (i.e., P1 in Fig. 2). As a result, the gap distance of R1, which is the longitudinal relative distance between R1 and its front vehicle, instantly increases. R1, which has gained the ideal reachable space, should first accelerate appropriately to catch up with the front vehicle, then slow down after approaching, and finally maintain an appropriate following distance. The same applies to the vehicles behind R1, who must perform similar accelerate-decelerate behavior to maintain the original longitudinal relative distance. The rear vehicles in the current lane that show an increasing-decreasing trend of gap distance after SV changes lane are considered to be affected by the SV's lane change.

- Target lane: in the opposite with the pattern of the current lane, the affected vehicles should show a decreasing-increasing trend in the gap distance in the target lane. This is because the gap distance of the vehicle immediately behind SV in the target lane (represented as R1') rapidly decreases due to SV's cut-in behavior. Consequently, R1' must first slow down to avoid a rear-end collision with SV, and then accelerate appropriately to restore the appropriate following distance.

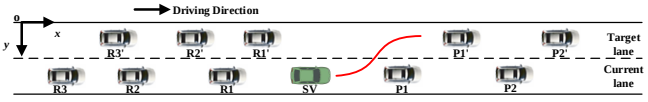

Fig. 2. Diagram of a lane change scenario

In the paper, the moment of lane change of SV (represented as t_{LC}) is defined as the moment when the center of the rear axle of SV passes the lane line. To avoid the effect of errors caused by data fluctuations, polynomials were fitted to the gap distance of each rear vehicle from 5 seconds before t_{LC} to 13 seconds after t_{LC} (i.e., time range $t \in [t_{LC}-5, t_{LC}+13]$, represented as [0,18] in the following text and figures). The fitted gap distance profiles of the rear vehicles of SV ($i = 1,2,3,\ldots$, ordered from the closest to farthest from SV) will be examined individually to determine if they are affected by SV's lane change. Once a vehicle is determined to be unaffected, the assessment is

terminated, and the vehicles behind it are considered unaffected. As the variation pattern in the gap distance of rear vehicles differs in the current and target lanes, they are investigated separately. Taking the current lane as an example, as illustrated in Fig. 3, vehicle i is deemed affected by SV's lane change if it satisfies all of the following conditions:

(1) Increasing trend condition: the fitted gap distance profile of vehicle i first exhibits an increasing trend when $t \in (t_{up,i}, t_{down,i})$. $t_{up,i}$ and $t_{down,i}$ refer to the start and end moments of the increasing trend after the reaction moment of the previous vehicle $i-1$, respectively (see Fig. 4). Specifically, $t_{up,i}$ is defined as the reaction moment of rear vehicle i under the lane change impact. For the 1st affected rear vehicle, the reaction moment $t_{up,1}$ is set to t_{LC} when an increasing trend starts before SV changes lane. Considering the driver's reaction time, an increasing trend should be observed in the fitted gap distance of each affected rear vehicle ($i = 2,3,...$) within 1s after the front vehicle reacts, as shown in Eq. (1). Any increase in the fitted gap distance profile beyond this time range is considered to be unaffected by the lane change.

$$d_{i,t+1} > d_{i,t}, t_{up,i} < t < t_{down,i} \quad \&t_{up,i-1} \le t_{up,i} \le t_{up,i-1} + 1 \tag{1}$$

where t refers to the time step (with the step size at 0.1s in the paper), $d_{i,t}$ is the fitted gap distance of the rear vehicle i in the current lane at time step t.

(2) Decreasing trend condition: when $t \in (t_{down,i}, t_{end,i})$, the fitted gap distance profile shows a decreasing trend, as shown in Eq. (2). $t_{down,i}, t_{end,i}$ are the start and end moments of the decreasing trend, respectively.

$$d_{i,t+1} < d_{i,t}, t_{down,i} < t < t_{end,i} \le t_{LC} + 13 \tag{2}$$

(3) Profile stability condition: when $t \in (t_{LC}, t_{LC} + 13)$, the curvature of the fitted gap distance profile should maintain stable, i.e., the difference of the fitted gap distance between neighboring time steps should be within a certain range, as shown in Eq. (3). Otherwise, it may indicate that the speed difference between the rear vehicle i and its front vehicle $i-1$ is large, and the change in gap distance is more likely to be affected by other hard-to-estimate influences compared with the influence of lane change.

$$\left|d_{i,t+1} - d_{i,t}\right| < th_1, t_{LC} < t \le t_{LC} + 13 \tag{3}$$

where $d_{i,t+1}$ and $d_{i,t}$ are the gap distance of the rear vehicle i at time $t+1$ and t respectively; th_1 is the convergence coefficient, and the recommended value is 1.

(4) Fluctuation stability condition: when $t \in (t_{LC}, t_{LC} + 13)$, the fluctuation of the fitted gap distance profile needs to be stable, i.e., the variation in the fitted gap distance of the rear vehicle i is within a certain range, as shown in Eq. (4). This is because the gap distance of the rear vehicle before SV changes lane is the distance that the driver tends to maintain. A large deviation from the intended gap distance may indicate that the rear vehicle is more likely to be influenced by other factors rather than a lane change.

$$\left|d_{i,LC} - d_{i,t}\right| < th_2, t_{LC} < t \le t_{LC} + 13 \tag{4}$$

where $d_{i,LC}$ is the gap distance of rear vehicle i at the moment when SV changes lane, $d_{i,t}$ is the gap distance of rear vehicle i at any moment, th_2 is the fluctuation coefficient, and the recommended value is 30. Note that the recommended values of th_1 and th_2 were obtained empirically from our several experiments based on the given dataset as described in Section V.

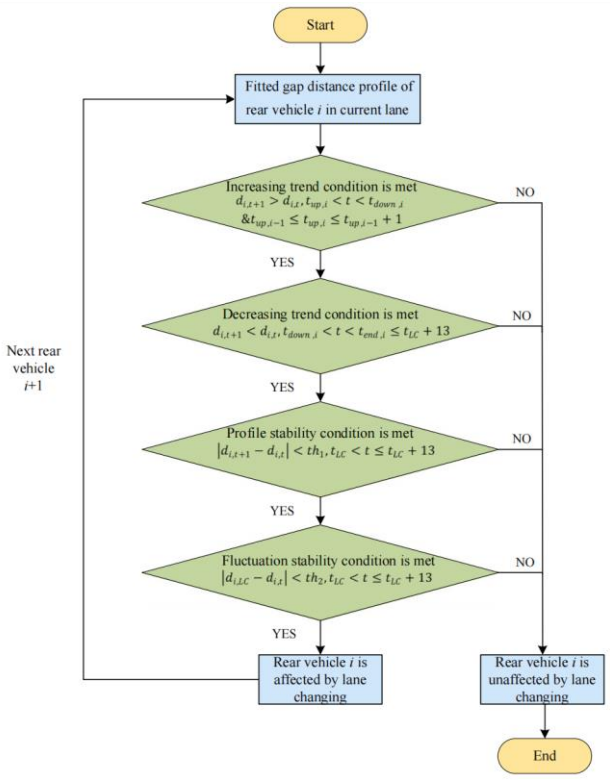

Fig. 3. Judgement process for affected vehicles in the current lane

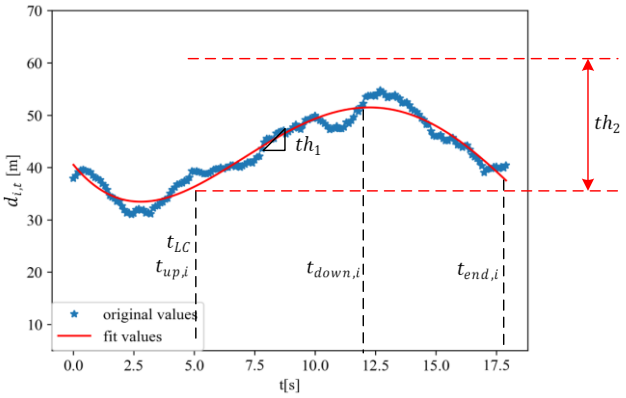

Fig. 4. An example fitted gap distance profile of rear vehicle i in the current lane

B. Ordered probit regression model

To predict the number of vehicles affected by SV's lane changing, an ordered probit regression model [38] is constructed using the explanatory variables listed in Table 1 to account for the potential differential impact of lane changing in varying traffic flow conditions. The number of affected vehicles in the current lane and the target lane are represented as I_{ego} and I_{tar}, respectively. It should be noted that all the explanatory variables are calculated at the moment when SV starts to change lane (i.e., the starting

moment of a continuous change in the lateral position of SV).

Table 1. Description of explanatory variables

Variables	Description
$Q_{egolane}$	Traffic density of current lane within 500 meters before and after SV (veh/km)
$avgV_{egolane}$	Average traffic speed of current lane within 500 meters before and after SV(m/s)
$Q_{tarlane}$	Traffic density of target lane within 500 meters before and after SV (veh/km)
$avgV_{tarlane}$	Average traffic speed of target lane within 500 meters before and after SV(m/s)
dV_{p1}	Speed difference between SV and the preceding vehicle in the current lane (m/s)
dV_{r1}	Speed difference between SV and the rear vehicle in the current lane (m/s)
$dV_{p1'}$	Speed difference between SV and the preceding vehicle in the target lane (m/s)
$dV_{r1'}$	Speed difference between SV and the rear vehicle in the target lane (m/s)
dD_{p1}	Distance between SV and the preceding vehicle in the current lane (m)
dD_{r1}	Distance between SV and the rear vehicle in the current lane (m)
$dD_{p1'}$	Distance between SV and the preceding vehicle in the target lane (m)
$dD_{r1'}$	Distance between SV and the rear vehicle in the target lane (m)
V_{sv}	Speed of SV (m/s)

In the paper, the number of affected vehicles in the lane-changing event is modeled as ordered variables. Taking the target lane as an example, the number of affected vehicles is divided into a total of six levels, i.e. $I_{tar} = 1,2,\dots,6$, where $I_{tar} = 1{\sim}5$ indicates that the number of affected vehicles in the rear traffic is $1{\sim}5$, respectively, and $I_{tar} = 6$ represents the number of affected vehicles is at least 6, as shown in Eq. (5).

$$I_{tar} = \begin{cases} 1, y < c_1 \\ 2, c_1 \le y < c_2 \\ 3, c_2 \le y < c_3 \\ 4, c_3 \le y < c_4 \\ 5, c_4 \le y < c_5 \\ 6, \quad y \ge c_5 \end{cases} \tag{5}$$

where y is a latent variable, the ordered variable I_{tar} is the observed value of y, and c_k is the threshold for evaluating the ordered variable. Specifically, a linear regression model is used to describe the relationship between the latent variable y and the explanatory variable vector $\boldsymbol{x}$, as shown in Eq. (6).

$$y = \beta_0 + \boldsymbol{\beta_1 x} + \varepsilon \tag{6}$$

where β_0 and $\boldsymbol{\beta_1}$ are regression coefficients, and ε is a disturbance term.

Finally, the ordered probit regression model can be established in Eqs. (7)-(8).

$$P(nums \le k) = F_\varepsilon(\alpha_k - \boldsymbol{\beta_1 x}) \tag{7}$$

$$\alpha_k = c_k - \beta_0 \tag{8}$$

where $nums$ represents the predicted number of affected vehicles (i.e., I_{ego} and I_{tar}), $F_\varepsilon(t)$ is the distribution function of ε, and is assumed to be a standard normal distribution in the paper, α_k represents the intercept.

Note that the ordered probit model was chosen to predict I_{ego} and I_{tar} because of its ease of interpretation in analyzing the correlation between the impact range and various factors, as well as its high computational efficiency in online applications. Furthermore, the focus of this paper is to demonstrate the effectiveness of the proposed trajectory planning algorithm (to be presented in detail in Section IV) using an easily applicable impact range prediction model; in the future, more accurate learning-based methods can be investigated to improve the prediction performance on lane change impacts.

IV. A LANE-CHANGING TRAJECTORY PLANNING ALGORITHM CONSIDERING THE INFLUENCE RANGE OF LANE-CHANGING

Gipps [39] first proposed a three-stage lane-changing model to describe the lane-changing process, i.e., the lane-changing intention generation stage, the gap acceptance stage, and the execution stage. This paper focuses on the final execution stage, specifically on how CAV lane-changing trajectory planning can reduce the impact of SV on the traffic flow while ensuring driving safety. It is assumed that SV has made a lane-changing decision because it is impeded by the slower vehicle in front of it. To overcome the limitations of previous studies, we propose a quintic polynomial-based lane-changing trajectory planning model that considers the influence range of lane changes.

A. Quintic polynomial trajectory planner

Considering the advantages of continuous third-order derivatives and smooth curvature, the quintic polynomials of longitudinal and lateral positions with respect to time are used in the paper to describe the trajectories of lane changing as shown in Eqs. (9)-(11).

$$\begin{cases} x(t) = a_0 + a_1 t + a_2 t^2 + a_3 t^3 + a_4 t^4 + a_5 t^5 \\ y(t) = b_0 + b_1 t + b_2 t^2 + b_3 t^3 + b_4 t^4 + b_5 t^5 \end{cases} \tag{9}$$

$$\begin{cases} \dot{x}(t) = a_1 + 2a_2 t + 3a_3 t^2 + 4a_4 t^3 + 5a_5 t^4 \\ \dot{y}(t) = b_1 + 2b_2 t + 3b_3 t^2 + 4b_4 t^3 + 5b_5 t^4 \end{cases} \tag{10}$$

$$\begin{cases} \ddot{x}(t) = 2a_2 + 6a_3 t + 12a_4 t^2 + 20a_5 t^3 \\ \ddot{y}(t) = 2b_2 + 6b_3 t + 12b_4 t^2 + 20b_5 t^3 \end{cases} \tag{11}$$

where $a_0, a_1, a_2, a_3, a_4, a_5, b_0, b_1, b_2, b_3, b_4, b_5$ are the unknown coefficients of the trajectory function, t refers to the time of the lane-changing process, and is within the range $t_s \le t \le t_f$. t_s is the starting moment of the lane-changing process, t_f is the ending moment of the lane-changing process. $x(t), \dot{x}(t), \ddot{x}(t), y(t), \dot{y}(t), \ddot{y}(t)$ are the longitudinal and lateral positions, velocities, and accelerations, respectively, of SV during the lane-changing process.

A total of 12 boundary conditions of longitudinal, lateral position, velocity, and acceleration at the start and end moments of lane changing were used to solve the polynomials. Considering the characteristics of the lane change scenario, the lane change starting moment is set to 0s, and the longitudinal acceleration, lateral velocity, and lateral acceleration of SV at the start and end moments of the lane change are assumed to be zero. At the end moment of lane changing, the lateral displacement is the lane width W, and the longitudinal velocity is the traffic velocity of the

target lane (represented as $v_{tarlane,flow}$). The equations are derived as in Eqs. (12)-(13).

$$\begin{cases} x(0) = 0, & \dot{x}(0) = v_{x,s}, & \ddot{x}(0) = 0 \\ y(0) = 0, & \dot{y}(0) = 0, & \ddot{y}(0) = 0 \end{cases} \tag{12}$$

$$\begin{cases} x(t_f) = x_f, & \dot{x}(t_f) = v_{tarlane,flow}, & \ddot{x}(t_f) = 0 \\ y(t_f) = W, & \dot{y}(t_f) = 0, & \ddot{y}(t_f) = 0 \end{cases} \tag{13}$$

As a result, the parameters to be determined in the quintic polynomial are the duration t_f and the longitudinal position x_f.

B. Benefit cost of rear vehicles

To quantify the potential impact of SV on the traffic flow behind it during lane changing, the Intelligent Driver Model (IDM) is used to characterize the driving behavior of the following vehicles in both the current and target lanes, as shown in Eqs. (14)-(15).

$$a_n(t) = a_0\left(1 - \left(\frac{v_n(t)}{v_0}\right)^4 - \left(\frac{s_n^*(t)}{s_n(t)}\right)^2\right) \tag{14}$$

$$s_n^*(t) = s_0 + Tv_n(t) + \frac{v_n(t)\Delta v(t)}{\sqrt{2a_0 b}} \tag{15}$$

where a_0 and v_0 are the maximum acceleration and desired velocity of the n^{th} following vehicle in the free stream, $v_n(t)$ is the velocity of the vehicle at time t, $s_n^*(t)$ is the desired headway, $s_n(t)$ is the actual headway, s_0 is the minimum headway, T is the safe time headway, $\Delta v(t)$ is the difference in the velocity of the vehicle and its preceding vehicle, and b is the comfort reduction velocity.

Take the cost function of the rear vehicle in the target lane as an example. Based on the predicted number of affected rear vehicles in the target lane I_{tar} and IDM model, the cost function of the rear vehicle in the target lane $J_{tarlane}$ can be calculated as shown in Eqs. (16)-(18).

$$J_{tarlane,c} = \sum_{i=1}^{I_{tar}} \omega_{tarlane_i} * J_{tarlane_i,c} \tag{16}$$

$$J_{tarlane,e} = \sum_{i=1}^{I_{tar}} \omega_{tarlane_i} * J_{tarlane_i,e} \tag{17}$$

$$J_{tarlane} = \omega_c * J_{tarlane,c}{}' + \omega_e * J_{tarlane,e}{}' \tag{18}$$

where $J_{tarlane,c}$ and $J_{tarlane,e}$ are the comfort cost function and efficiency cost function of the rear traffic in the target lane. ω_c and ω_e are the weights of the comfort cost function and efficiency cost function. $'$ denotes normalization. $tarlane_i = 1,2,\dots,I_{tar}$ denotes the rear vehicles in the target lane within the predicted impact range of lane changing from section III, ordered from the smallest to the largest longitudinal relative distance to SV. The comfort cost function and efficiency cost function of each vehicle, $J_{tarlane_i,c}$ and $J_{tarlane_i,e}$, are calculated as in Eqs. (19)-(20), respectively.

$$J_{tarlane_i,c} = \int_{t_s}^{t_f} \left| j_{tarlane_i}(t) \right| dt \tag{19}$$

$$J_{tarlane_i,e} = \int_{t_s}^{t_f} \left| \dot{x}_{tarlane_i}(t_s) - \dot{x}_{tarlane_i}(t) \right| dt \tag{20}$$

where $j_{tarlane_i}(t)$ and $\dot{x}_{tarlane_i}(t)$ denote the longitudinal jerk and velocity of the vehicle in the target lane, respectively.

$\omega_{tarlane_i}$ is the assigned weight of rear vehicle $tarlane_i$ in the target lane traffic. Rear vehicles with smaller longitudinal relative distances to SV should be weighted more heavily, as shown in Eqs. (21)-(22).

$$\tau_{tarlane_i} = \frac{1}{x(t_s) - x_{tarlane_i}(t_s)} \tag{21}$$

$$\omega_{tarlane_i} = \frac{\tau_{tarlane_i}}{\sum_{tarlane_i=1}^{I_{tar}} \tau_{tarlane_i}} \tag{22}$$

where $\tau_{tarlane_i}$ is the inverse of the initial longitudinal relative distance between $tarlane_i$ and SV.

The cost function of vehicles in the current lane $J_{egolane}$ is calculated in the same way.

C. Benefit cost of SV

The cost function of SV J_{SV} is calculated as Eqs. (23)-(25):

$$J_{SV} = \omega_c * J_{SV,c}{}' + \omega_{ef} * J_{SV,ef}{}' \tag{23}$$

$$J_{SV,c} = \int_{t_s}^{t_f} |\ddot{x}(t)|\, dt + \int_{t_s}^{t_f} |\ddot{y}(t)|\, dt \tag{24}$$

$$J_{SV,ef} = t_f - t_s \tag{25}$$

where $J_{SV,c}$ and $J_{SV,ef}$ are the comfort and efficiency costs of the SV. SV has the same comfort weight ω_c as rear vehicles. However, the efficiency weight of SV (ω_{ef}) should be distinguished from that of the rear vehicles (ω_e) due to the different analysis dimensions. $\ddot{x}$ and $\ddot{y}$ are the longitudinal and lateral jerk of the SV, respectively.

D. Potential risk cost

Based on the potential field theory, a predictive risk field model that combines spatial and temporal dimensions is proposed to characterize the potential risk of SV's interaction with the obstacles. By quantifying the trajectory risk, lane-changing trajectories that do not meet the safety conditions will be filtered out.

D1. Obstacle Vehicle Risk

The motion trajectories of surrounding obstacle vehicles are predicted through a constant acceleration model that features high prediction accuracy in a short time. The longitudinal and lateral displacement of the obstacle vehicles $\Delta x(\Delta t)$, $\Delta y(\Delta t)$ are predicted by Eqs. (26)-(27).

$$\Delta x(\Delta t) = v_x \Delta t + 0.5 a_x \Delta t^2 \tag{26}$$

$$\Delta y(\Delta t) = v_y \Delta t + 0.5 a_y \Delta t^2 \tag{27}$$

where v_x, v_y, a_x, a_y are the longitudinal and lateral velocities and accelerations and Δt refers to the time step.

Taking the center of gravity of the obstacle vehicle as the coordinate origin, the risk field $Risk_{veh}(t)$ posed by the obstacle vehicle can be calculated as Eq. (28) (as shown Fig.5) based on the proximity to the obstacle vehicle.

This article has been accepted for publication in IEEE Transactions on Intelligent Vehicles. This is the author's version which has not been fully edited and content may change prior to final publication. Citation information: DOI 10.1109/TIV.2024.3404658

$$Risk_{veh}(t)=\begin{cases}1, & |x(t)|\le x_{veh}\ and\ |y(t)|\le y_{veh}\ (Q1)\\ x_{mod}(t), & x_{cri}(t)>x(t)>x_{veh}\ and\ |y(t)|\le y_{veh}\ (Q2)\\ \psi x_{mod}(t), & -x_{veh}>x(t)>-x_{cri}(t) and\ |y(t)|\le y_{veh}\ (Q2')\\ y_{mod}(t), & y_{cri}(t)>y(t)>y_{veh}\ and\ |x(t)|\le x_{veh}\ (Q3)\\ \psi y_{mod}(t), & -y_{veh}>y(t)>-y_{cri}(t) and\ |x(t)|\le x_{veh}\ (Q3')\\ x_{mod}(t)*y_{mod}(t), & x_{cri}(t)>x(t)>x_{veh}\ and\ y_{cri}(t)>y(t)>y_{veh}\ (Q4)\\ \psi x_{mod}(t)*y_{mod}(t), & -x_{veh}>x(t)>-x_{cri}(t) and\ y_{cri}(t)>y(t)>y_{veh}\ (Q4'),\\ & x_{cri}(t)>x(t)>x_{veh}\ and\ -y_{veh}>y(t)>-y_{cri}(t)(Q4'),\\ & -x_{veh}>x(t)>-x_{cri}(t) and\ -y_{veh}>y(t)>-y_{cri}(t)(Q4')\\ 0, & x(t)\le -x_{cri}(t)\ or\ x(t)\ge x_{cri}(t) or\ y(t)\ge y_{cri}(t)\ or\ y(t)\le -y_{cri}(t)(Q5)\end{cases} \tag{28}$$

where x_{veh}, y_{veh} are the geometrical dimensions of the vehicle, $x_{mod}(t)$, $y_{mod}(t)$ are safety mitigation indices, which are monotonically decreasing functions that express the process of decreasing risk field of the obstacle vehicle with increasing longitudinal and lateral distances. $x_{cri}(t)$, $y_{cri}(t)$ are the critical longitudinal and lateral distances. ψ is the risk reduction coefficient, and a value of 1 means the same risk values in all directions (0.5 is taken in the paper).

The geometric dimensions of the vehicle x_{veh}, y_{veh} and the safety mitigation functions $x_{mod}(t)$, $y_{mod}(t)$ are calculated as Eqs. (29)-(32):

$$x_{veh}=\frac{1}{2}(lcos\theta+w|sin\theta|) \tag{29}$$

$$y_{veh}=\frac{1}{2}(wcos\theta+l|sin\theta|) \tag{30}$$

$$x_{mod}(t)=\frac{\left(x_{cri}-x(t)\right)^2}{(x_{cri}-x_{veh})^2} \tag{31}$$

$$y_{mod}(t)=\frac{\left(y_{cri}-y(t)\right)^2}{(y_{cri}-y_{veh})^2} \tag{32}$$

where l is the vehicle length, w is the vehicle width, and θ is the heading angle. $x_{cri}(t)$, $y_{cri}(t)$ represent the critical longitudinal and lateral distances beyond which no risk is assumed, and are calculated as Eqs. (33)-(34):

$$x_{cri}(t)=\begin{cases}cos\theta(x_{min}+\frac{1}{2}l), & v_{xr}(t)\le 0\\ cos\theta(\sigma_1|v_{xr}(t)|+x_{min}+\frac{1}{2}l), & v_{xr}(t)>0\ and\ |y_r(t)|\ge w\\ cos\theta(\sigma_1|v_{xr}(t)|+\sigma_2 e^{\frac{v_{xr}(t)+a_x(t)}{|x_r(t)|}}+x_{min}+\frac{1}{2}l), & v_{xr}(t)>0\ and\ |y_r(t)|<w\end{cases} \tag{33}$$

$$y_{cri}(t)=\begin{cases}(1+|sin\theta|)(y_{min}+\frac{1}{2}w), & v_{yr}(t)\le 0\\ (1+|sin\theta|)(\sigma_1|v_{yr}(t)|+y_{min}+\frac{1}{2}w), & v_{yr}(t)>0\ and\ |x_r(t)|\ge l\\ (1+|sin\theta|)(\sigma_1|v_{yr}(t)|+\sigma_2 e^{\frac{v_{yr}(t)+a_y(t)}{|y_r(t)|}}+y_{min}+\frac{1}{2}w), & v_{yr}(t)>0\ and\ |x_r(t)|<l\end{cases} \tag{34}$$

where the subscripts x and y denote the longitudinal and lateral directions, respectively. v_r is the relative velocity between the obstacle vehicle and SV. $v_r>0$ means that the direction of the relative velocity is pointed to SV. x_r, y_r are the longitudinal and lateral relative distances between the obstacle vehicle and SV. x_{min}, y_{min} are the minimum safe longitudinal and lateral vehicle distances. $a_x(t), a_y(t)$ are the longitudinal and lateral accelerations of the obstacle vehicle. σ_1, σ_2 are the preset parameters with recommended values of 0.9 and 0.8, respectively.

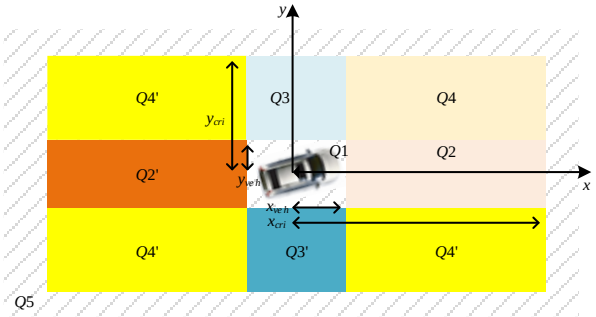

Fig. 5. Risk field posed by an obstacle vehicle

D2. Lane risk

The vehicle is exposed to an increasing degree of risk as it travels from the centre line of the lane to the lane line, as shown in Fig. 6, The lane risk field $Risk_{lane}(t)$ is calculated as Eq. (35) based on traffic rules.

$$Risk_{lane}(t)=-\left|Risk_{lane,max}*\sin\left(\frac{\pi y(t)}{W}\right)\right|+Risk_{lane,max} \tag{35}$$

where $Risk_{lane,max}$ is the preset maximum lane risk value, which represents the risk when the vehicle travels on the lane line, and W is the lane width.

In sum, the predicted risk field $Risk(t)$ in Fig. 7 is a combination of obstacle vehicle risk and lane risk, as shown in Eq. (36).

$$Risk(t)=\max\left(Risk_{veh}(t), Risk_{lane}(t)\right) \tag{36}$$

This article has been accepted for publication in IEEE Transactions on Intelligent Vehicles. This is the author's version which has not been fully edited and content may change prior to final publication. Citation information: DOI 10.1109/TIV.2024.3404658

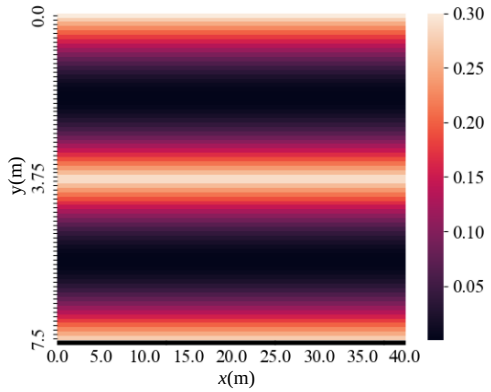

Fig. 6. Example lane risk field

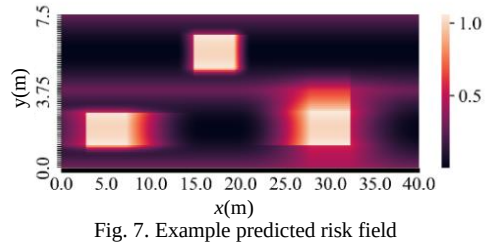

Fig. 7. Example predicted risk field

D3. Trajectory risk

Based on the established predictive risk field model, the trajectory safety cost function can be constructed. For each time step, 10 points are sampled uniformly in the longitudinal and lateral directions of the trajectory, and the maximum risk value $Risk_{max}$ and average risk value $Risk_{mean}$ of the trajectory are calculated as Eqs. (37)-(39).

$$Risk_{max} = \max\{\sum_{q=1}^{10} Risk(t)\left[\frac{q}{10}(x_{max}-x_{min}), \frac{q}{10}(y_{max}-y_{min})\right], t = 0,1,\dots,T\} \quad (37)$$

$$Risk_{mean} = \mathrm{mean}\{\sum_{q=1}^{10} Risk(t)\left[\frac{q}{10}(x_{max}-x_{min}), \frac{q}{10}(y_{max}-y_{min})\right], t = 0,1,\dots,T\} \quad (38)$$

$$T = \lceil t_f - t_s \rceil \quad (39)$$

where, x_{max}, y_{max}, x_{min}, y_{min} are the maximum and minimum positions of the trajectory in the longitudinal and lateral directions. q refers to the position of the sampling point. $Risk(t)[x,y]$ is the predicted risk of the sampling point located at the coordinate (x,y) at time t. $t = 0,1,\dots,T$ refers to the observed moments of the lane-changing process, where T is the round-up value of the duration of the lane change.

As high-risk trajectories may have safety problems during lane changing, the trajectories with high maximum risk need to be excluded. As a result, the maximum safety cost function J_{safe}^{max} is calculated as Eq. (40).

$$J_{safe}^{max} = \begin{cases} inf, & Risk_{max} \geq Risk_{max,preset} \\ 1, & Risk_{max} < Risk_{max,preset} \end{cases} \quad (40)$$

where $Risk_{max,preset}$ is the preset trajectory risk threshold. inf is an infinite value.

The average risk is also an important measure of trajectory safety, and is constructed as a cost function component as Eq. (41).

$$J_{safe}^{mean} = Risk_{mean} \quad (41)$$

E. Total cost function

The total cost function is established by combining the benefit costs of SV and the rear vehicles, as well their potential risk costs during lane change interaction, as shown in Eq. (42). Taking the kinematic constraints of the lane-changing trajectories into account, the lane-changing trajectory planning is finally transformed into a constrained optimization problem with two decision variables from the quintic polynomial planner (i.e., t_f and x_f), which can be solved using a genetic algorithm.

$$minJ(t_f, x_f) = J_{safe}^{max}(\omega_{SV} * J_{SV} + \omega_{egolane} * J_{egolane} + \omega_{tarlane} * J_{tarlane} + \omega_{safe} * J_{safe}^{mean}) \quad (42)$$

$$s.t.$$

$$|\dot{x}(t)| < v_{x,max}$$
$$|\dot{y}(t)| < v_{y,max}$$
$$|\ddot{x}(t)| < a_{x,max}$$
$$|\ddot{y}(t)| < a_{y,max}$$
$$|\dddot{x}(t)| < j_{x,max}$$
$$|\dddot{y}(t)| < j_{y,max}$$
$$t_{f,min} < t_f < t_{f,max}$$

where ω_{SV}, $\omega_{egolane}$, $\omega_{tarlane}$, ω_{safe} are the weights of the cost functions of SV, the rear vehicles in the current lane, the rear vehicles in the target lane, and average driving risk, respectively. $v_{x,max}$, $v_{y,max}$, $a_{x,max}$, $a_{y,max}$, $j_{x,max}$, $j_{y,max}$ are the maximum longitudinal and lateral velocities, acceleration and jerk, respectively. $t_{f,min}$, $t_{f,max}$ are the minimum and maximum end time of lane change.

V. RESULT

A. Data preprocessing

To predict the impact range of lane change, one lane change record should include the trajectories of SV and its *n* following vehicles in the current and target lanes before and after the lane change, as well as enough information to calculate the local traffic flow statistics needed to build the prediction model. Compared with other commonly used trajectory datasets such as NGSIM and highD, the road lengths recorded in the Zen Traffic Data [40] are generally longer, which can better meet the data requirements of the lane change impact range analysis and was therefore used in the paper. The study site of the Zen Traffic Data is an approximately 2-kilometer section of the Hanshin Expressway Line 11 Ikeda Line (Osaka direction) near the Tsukimoto intersection in Japan, as shown in Fig. 8. The dataset consists of five one-hour vehicle trajectory data in the morning peak period, and approximately 100% of the trajectories of all vehicles in the target road section are covered at a frequency of 0.1s. The dataset was preprocessed through the following steps, resulting in a total of 411 trajectory samples.

(1) Extracting the trajectory of a lane-changing vehicle, the trajectories of its 10 following vehicles in the current and target lanes before and after the lane change, and the local traffic flow statistics at the moment of lane change as a lane-changing sample;

(2) Removing samples with lane-changing behavior occurred in the rear vehicles after SV changes lane. This is to avoid overly complex coupling issues that may be caused by allowing the rear vehicles to change lanes;

(3) Removing samples of continuous lane changing (i.e., SV continuously crosses two or more lanes). Continuous lane changing is a more complex behavior that can cause a larger impact on the rear traffic, and is not considered in the paper;

(4) Removing samples with less than 13 seconds of trajectory for SV or rear vehicles after the lane change moment;

(5) Removing samples that involve entering and exiting from the ramp to exclude the impact of forced lane changes.

Fig. 8. Study area of the Zen Traffic Data

B. Influence range of lane changing

The extracted lane-changing trajectory samples were analyzed based on the proposed evaluation scheme in Section III-A to assess the influence range of lane change. Fig.9 shows example fitted gap distance curves of the rear vehicles in the current and target lanes of SV.

- Current lane: As shown in Fig. 9(d), although the fitted gap distance curve of the 4th rear vehicle in the current lane conforms to the increasing-decreasing trend, it fluctuates too much and does not meet the condition of curve fluctuation stability, and thus is considered not being affected by SV's lane change. This can also be explained from a driver's behavioral perspective, that is if the 4th rear vehicle in the current lane is affected by the lane change, it should try to maintain the same gap distance before and after SV's lane change (i.e., lane change does not make conservative/ aggressive drivers become aggressive/ conservative); however, the gap distance is significantly higher after SV's lane change. Compared with the impact of lane changing, the fluctuation in the gap distance of the 4th rear vehicle in the current lane is more likely to be affected by other factors, such as the speeds and distances of its neighboring vehicles on the left and right, complex driving behavioral habits, psychological impacts, etc. As a result, the number of affected vehicles in the current lane is determined to be 3.

- Target lane: As shown in Fig. 9(f), the 2nd rear vehicle in the target lane reacts at 5.2s and satisfies all conditions. In Fig. 9(g), although the gap distance of the 3rd rear vehicle in the target lane shows a decreasing-increasing profile, it starts to decrease at 7.3s (which is about 2s later than the 2nd rear vehicle reacts) and does not meet the preset 1s reaction time assumption in the decreasing trend condition for the target lane. As a result, the 3rd rear vehicle is assumed to be only slightly or negligibly affected by the lane change, and the number of affected vehicles in the target lane is determined to be 2.

This article has been accepted for publication in IEEE Transactions on Intelligent Vehicles. This is the author's version which has not been fully edited and content may change prior to final publication. Citation information: DOI 10.1109/TIV.2024.3404658

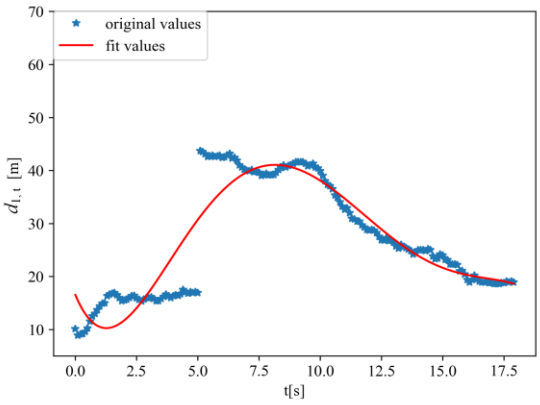

(a) 1st rear vehicle in the current lane

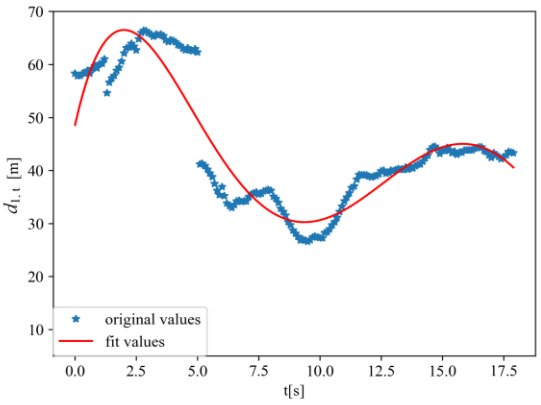

(e) 1st rear vehicle in the target lane

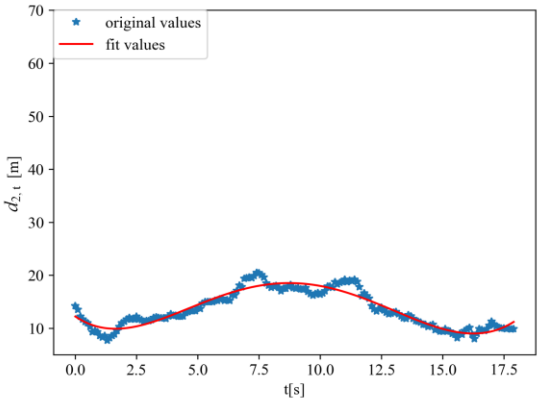

(b) 2nd rear vehicle in the current lane

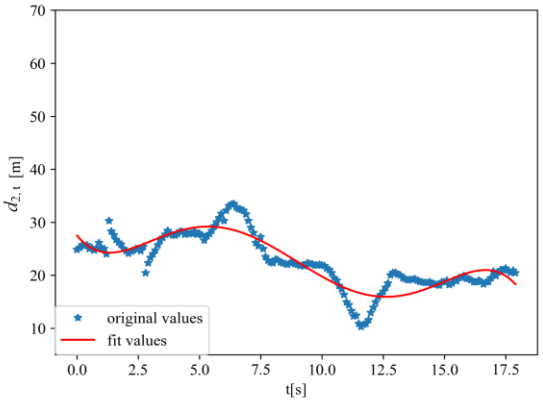

(f) 2nd rear vehicle in the target lane

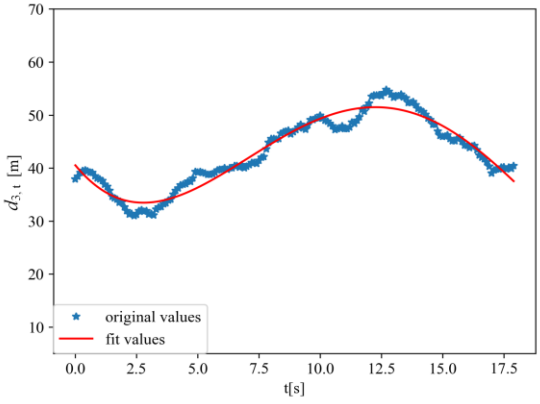

(c) 3rd rear vehicle in the current lane

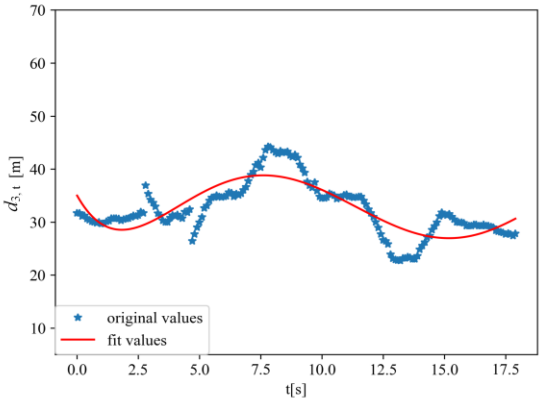

(g) 3rd rear vehicle in the target lane

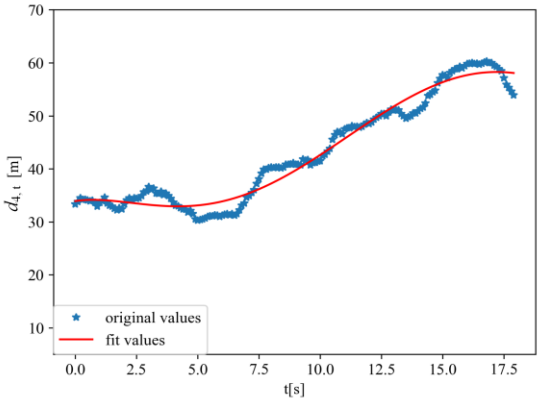

(d) 4th rear vehicle in the current lane

Fig. 9. Example fitted gap distance curves of the rear vehicles in the current and target lanes of SV

This article has been accepted for publication in IEEE Transactions on Intelligent Vehicles. This is the author's version which has not been fully edited and content may change prior to final publication. Citation information: DOI 10.1109/TIV.2024.3404658

Based on the number of affected rear vehicles by lane change obtained above, an ordered probit regression model was estimated for lane change impact range prediction as described in Section III-B. In the paper, there are a total of 13 candidate variables that may affect the number of vehicles influenced by lane changing. To prevent the existence of a strong correlation between the variables that can lead to biased results, it is necessary to reduce multicollinearity within the variables. VIF, tolerance, and conditional index were adopted to test the covariance of independent variables, and the results are shown in Table 2. VIF is the ratio of the variance of the explanatory variables when there is multicollinearity to that when there is no multicollinearity [41]. Tolerance is the proportion of residuals obtained when each independent variable is modeled as the dependent variable in a regression on the other independent variables. Conditional index is an index calculated from the eigenvalues. Previous research shows that there can be serious multicollinearity between variables when VIF is greater than 10 and tolerance is less than 0.1. In addition, when the maximum value of the conditional index is higher than 100, a serious multicollinearity may exist and it is unsuitable for regression analysis. Based on the values of the above-mentioned indices presented in Table 2, three variables including V_{SV}, $avgV_{egolane}$, and $avgV_{tarlane}$ were considered to have serious multicollinearity problem, and were excluded from the subsequent ordered probit regression analysis.

Table 2. Collinearity diagnostics

Variable	Tolerance	VIF	Eigenvalue	Condition Index
V_{sv}	0.068	14.733	1.850	2.139
dD_{p1}	0.610	1.639	1.254	2.598
dV_{p1}	0.434	2.303	0.616	3.707
dD_{r1}	0.675	1.483	0.497	4.129
dV_{r1}	0.673	1.486	0.367	4.802
$dD_{p1'}$	0.552	1.811	0.307	5.249
$dV_{p1'}$	0.349	2.867	0.253	5.790
$dD_{r1'}$	0.733	1.364	0.192	6.638
$dV_{r1'}$	0.307	3.262	0.147	7.595
$Q_{egolane}$	0.482	2.074	0.035	15.656
$avgV_{egolane}$	0.061	16.486	0.008	33.207
$Q_{tarlane}$	0.444	2.250	0.005	42.313
$avgV_{tarlane}$	0.099	10.079	0.004	47.868

Take the analysis of the number of affected vehicles in the current lane as an example. The relevant fitting/assumption test results of the ordered probit model are presented in Table 3 to Table 5. As can be seen from the model fit information table in Table 3, the *p*-value is much less than 0.05, indicating that the intercept-only model cannot be accepted and that at least one of the explanatory variables is significantly correlated with the response variable. In Table 4, the *p*-value of both the Pearson χ^2 goodness-of-fit test and the deviance goodness-of-fit test are greater than 0.95, meaning the null hypothesis that the model can well fit the observation data holds. In Table 5, the *p*-value of 0.986 is much greater than 0.05, meaning the parallel regression assumption is not violated and the problem is suitable to be solved using the ordered regression model. In sum, the ordered probit regression model constructed in this paper passes the goodness-of-fit and parallel regression assumption tests, and the regression results have strong explanatory significance. Detailed model regression results are presented in Table 6.

Table 3. Model fitting information

Hypothesis	-2 *log-likelihood*	χ^2	d.f.	*p*-value
Intercept Only	1449.250			
Full Model	1421.034	28.216	10	0.002

Table 4. Goodness-of-fit test

Statistic	χ^2	d.f.	*p*-value
Pearson	2048.545	2040	0.953
Deviance	1421.034	2040	1.000

Table 5. Test of parallel regression assumption

Hypothesis	-2 *log-likelihood*	χ^2	d.f.	*p*-value
Null	1421.034			
Alternative	1398.023	23.011	40	0.986

As shown in Table 6, dV_{r1} (the speed difference between SV and the rear vehicle in the current lane at the moment of lane change) and $Q_{egolane}$ (the traffic density of the current lane within 500 meters before and after SV) are both significant at the 0.05 level, and their coefficient estimates are both positive. This indicates that the higher the two variables are, the higher the number of affected vehicles in the current lane is affected, which is in accordance with what one would expect. Table 7 shows the percentage prediction error of the ordered probit regression model in predicting the number of affected vehicles in the current lane. In the paper, prediction error refers to the difference between the actual number of affected vehicles and the model estimate. The percentage of samples with prediction error within one is 72%, which indicates that the overall prediction performance of the established model is good and the predicted range of lane-changing influence can be fed into the lane-changing trajectory planning algorithm considering the benefits of surrounding vehicles.

This article has been accepted for publication in IEEE Transactions on Intelligent Vehicles. This is the author's version which has not been fully edited and content may change prior to final publication. Citation information: DOI 10.1109/TIV.2024.3404658

Table 6. Parameter estimates

		Estimate	Std. Err	Wald Stat.	d.f.	Sig.	95%Confidence Interval Lower Bound	Upper Bound
Threshold	[I_{ego} = 1]	-0.670	0.533	1.579	1	0.209	-1.716	0.375
	[I_{ego} = 2]	0.337	0.532	0.402	1	0.526	-0.705	1.379
	[I_{ego} = 3]	0.965	0.534	3.272	1	0.070	-0.081	2.011
	[I_{ego} = 4]	1.547	0.537	8.291	1	0.004	0.494	2.599
	[I_{ego} = 5]	2.255	0.544	17.175	1	0.000	1.188	3.321
Variables	dD_{p1}	-0.008	0.006	2.163	1	0.141	-0.019	0.003
	dV_{p1}	-0.030	0.018	2.940	1	0.086	-0.064	0.004
	dD_{r1}	0.003	0.003	0.709	1	0.400	-0.004	0.010
	dV_{r1}	0.054	0.017	9.628	1	0.002	0.020	0.088
	dD_{p1},	0.003	0.003	0.576	1	0.448	-0.004	0.009
	dV_{p1},	0.021	0.016	1.693	1	0.193	-0.010	0.051
	dD_{r1},	-0.005	0.004	1.579	1	0.209	-0.012	0.003
	dV_{r1},	-0.011	0.015	0.523	1	0.470	-0.041	0.019
	$Q_{egolane}$	0.028	0.011	6.958	1	0.008	0.007	0.049
	$Q_{tarlane}$	-0.005	0.009	0.303	1	0.582	-0.023	0.013

Table 7. Model prediction results

Prediction error	Percentage（%）
0	39
1	33
2	15
3	7
4	6

C. Verification of lane change trajectories

To verify the effectiveness of the proposed lane-changing trajectory algorithm, the performance of different lane-changing algorithms are compared in terms of trajectory efficiency and safety. A simulation environment for a lane-changing scenario on a straight two-lane road has been constructed using the Simulation of Urban Mobility (SUMO) platform with a Python TraCI interface. Specifically, fifteen vehicles are traveling on each lane with an initial gap distance of 60m and an initial speed of 15m/s. Such initial conditions are intended to prevent collisions while presenting a typical scenario of dense traffic. The vehicles are uniformly set as a passenger car with a length of 4.5m and a width of 2.2m, and the default Krauss model is employed to control their car-following behavior.

C1. Lane change efficiency

The efficiency improvement of the proposed algorithm was verified from SV and rear vehicle trajectories, respectively.

(1) SV trajectories

Fig. 10 shows the lane-changing trajectories of SV generated by four different lane-changing algorithms, where the green line represents the general algorithm that focuses solely on the benefits of SV [15], the orange line represents our proposed algorithm that integrates the benefits of SV and the predicted affected rear vehicles, the blue line represents the baseline algorithm that focuses on the benefits of the 10 rear vehicles in the target lane [6], and the grey line represents the locally optimal version of our algorithm that solely considers the predicted affected rear vehicles.

As can be seen from Fig. 10, the general algorithm has the shortest lane-changing duration, with larger lateral velocity/acceleration/jerk and smaller longitudinal velocity/acceleration/jerk. Deceleration also occurs during lane changing, which may have an adverse effect on the vehicles behind. This is because the general algorithm solely focuses on the efficiency and comfort of SV in lane changing, i.e., allowing SV to change lanes quickly while minimizing speed fluctuations. Conversely, the locally optimal algorithm that focus solely on the efficiency of surrounding vehicles tends to produce more stable lateral performance and higher longitudinal acceleration (which are beneficial in reducing the lane change impact of SV on traffic and in increasing the overall traffic flow speed), however with longer lane-changing duration of SV. The trajectory indices of the proposed algorithm and the baseline algorithm fall between those of the general algorithm and the locally optimal algorithm. Compared with the baseline algorithm, our proposed algorithm achieves shorter lane-changing time and higher longitudinal speed and acceleration.

(2) Rear vehicle trajectories

Fig. 11 (a) and (b) show the trajectories of 10 rear vehicles in the current and target lanes during the entire simulation using the general algorithm, while (c) and (d) correspond to our proposed algorithm.

- Rear vehicles in the current lane: As can be seen in Fig. 11(a), the two nearest rear vehicles in the current lane under the general algorithm show a deceleration process when SV starts to change lane (t=5s in the figure), indicating they are affected by the lane change and need to decelerate to maintain a safe following distance. In Fig. 11(c), the rear vehicles in the current lane keep accelerating during the lane change of SV. This indicates that our algorithm can improve the driving speed of the rear vehicles by increasing the longitudinal speed of SV in lane changing, and thus reduce the lane change impact on the rear vehicles.

- Rear vehicles in the target lane: Stimulated by the SV's lane-changing cut-in behavior, the rear vehicle closest to SV in the target lane shows a deceleration-acceleration trajectory to maintain a reasonable following distance. The deceleration rates of the first and second rear vehicles in the

This article has been accepted for publication in IEEE Transactions on Intelligent Vehicles. This is the author's version which has not been fully edited and content may change prior to final publication. Citation information: DOI 10.1109/TIV.2024.3404658

target lane are (3.00m/s^2, 0.21 m/s^2) for the general algorithm and (1.68 m/s^2, 0.13 m/s^2) for our proposed algorithm. This indicates that our algorithm results in lower deceleration rates of the rear vehicles compared with the general algorithm, and can reduce the impact of lane change on the rear vehicles in the target lane.

In sum, the proposed lane-changing trajectory planning algorithm avoids excessive speed fluctuations in the rear vehicles, and can maintain more stable trajectories during the lane change of SV. To further assess the impact of lane changing on the rear vehicles, the speed change rates [42] of the vehicles in the current and target lanes were calculated as shown in Eq. (43).

$$speed\ \ change\ \ rate_i = \frac{\left|v_{end,i} - v_{start,i}\right|}{v_{start,i}} * 100\% \quad (43)$$

where $v_{start,i}$ and $v_{end,i}$ represent the speed of the rear vehicle i at the beginning and end of SV's lane change, respectively. This indicator actually illustrates the speed increase in the current lane due to SV's leaving and the speed decrease in the target lane caused by SV's cut-in. A higher speed increase rate and a lower speed decrease rate suggest a smaller impact of the lane change on the efficiency of local traffic.

Table 8 presents the 150-metre travel time, 15-second travel distance, the maximum acceleration and speed increase rate of the rear vehicles in the current lane, and the maximum deceleration and speed decrease rate of the rear vehicles in the target lane during lane change using the four algorithms. It can be seen that the rear vehicles under the local optimal algorithm have the shortest travel time and longest travel distance in both the current and target lanes, as well as the smallest maximum deceleration and speed decrease rate in the target lane. This indicates that compared with other algorithms, the lane-changing trajectory that only considers the benefits of the surrounding vehicles can facilitate high-speed cut-in and reduce the negative impact on the rear vehicles. However, as discussed in the previous section, it tends to prolong the duration of lane change and sacrifices the benefits of SV. When compared with the baseline algorithm, the 150-metre travel time of the first three rear vehicles under our algorithm is 0.1~0.2s shorter. Also, our algorithm has a higher speed increase rate in the current lane and a lower speed decrease rate in the target lane, indicating it can effectively evaluate the benefits of SV and the surrounding vehicles and improve the local traffic speed. The results demonstrate although the baseline algorithm considers the benefits of 10 rear vehicles in the target lane, the lane-changing impact range may not be so large and more vehicles have been taken into account than necessary. In other words, such a static number of considered rear vehicles could lead to redundant and inefficient cost functions and even waste of computational resources. By first predicting the number of vehicles affected by the lane change, our algorithm can focus on the benefits of the influenced rear vehicles in the current and target lanes, and effectively increase the speed of traffic flow.

(3) Efficiency performance with different initial flow speed

The initial speed of the traffic flow was further changed to 25m/s and 35m/s, respectively, to verify the generalization of the proposed algorithm in different scenarios. Fig. 12 presents the efficiency improvement by the proposed algorithm compared with the baseline algorithm at different initial speeds of the traffic flow. The results show that compared with the baseline algorithm, the proposed algorithm can effectively reduce the speed decrease rate of the first rear vehicle in the target lane by 1.03%, 2.53%, and 3.26% at initial flow speeds of 15m/s, 25m/s, and 35m/s, respectively. These indicate that the proposed algorithm generally shows better performance in improving the driving efficiency of surrounding vehicles with different initial speeds, especially when the speed is higher.

This article has been accepted for publication in IEEE Transactions on Intelligent Vehicles. This is the author's version which has not been fully edited and content may change prior to final publication. Citation information: DOI 10.1109/TIV.2024.3404658

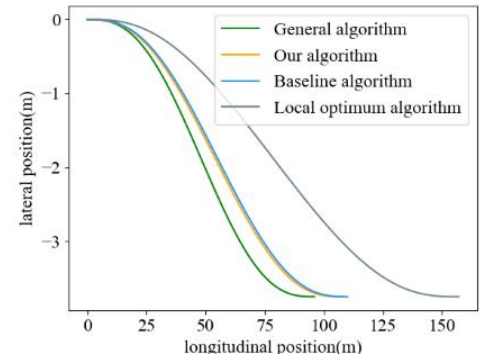

(a) position curve

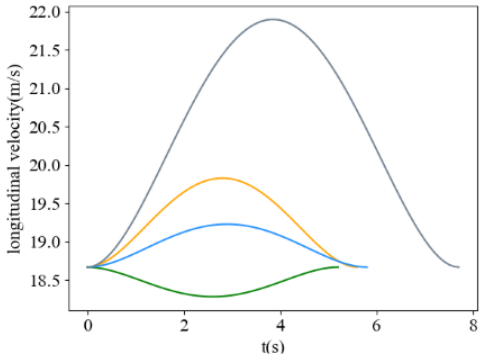

(b) longitudinal velocity curve

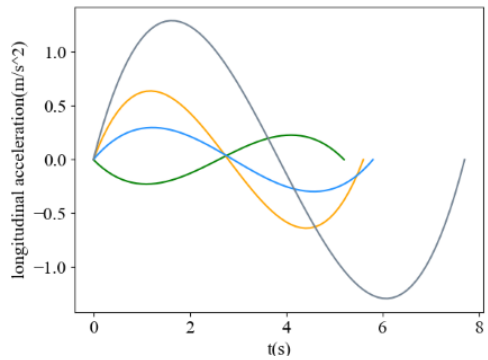

(c) longitudinal acceleration curve

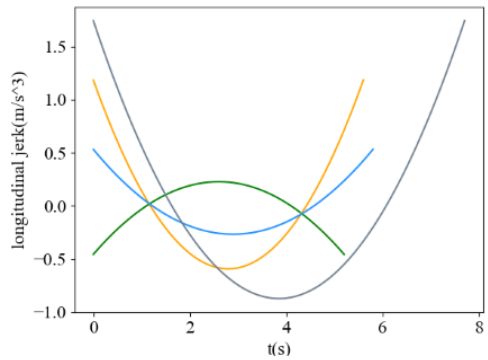

(d) longitudinal jerk curve

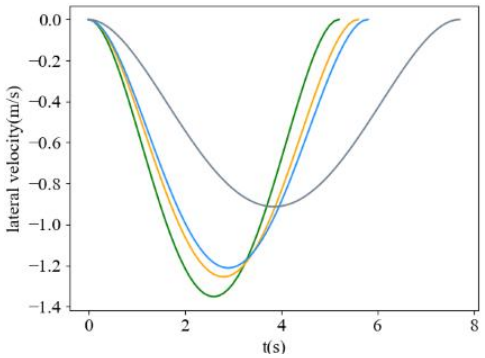

(e) lateral velocity curve

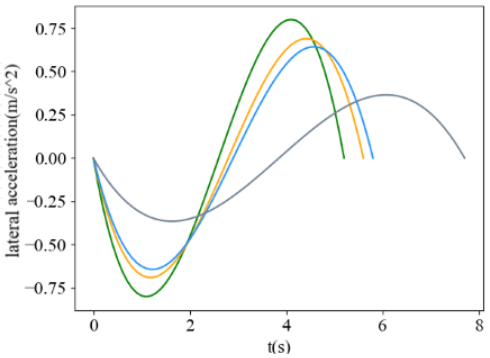

(f) lateral acceleration curve

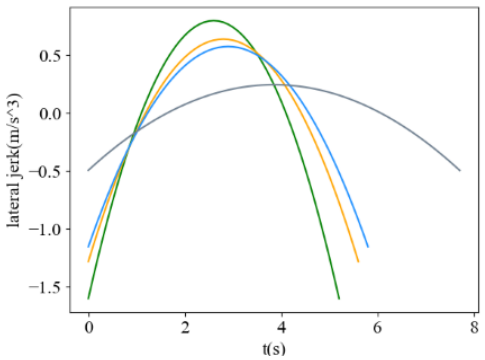

(g) lateraljerk curve

Fig. 10. Lane-changing trajectories of SV with an initial flow speed at 15m/s

This article has been accepted for publication in IEEE Transactions on Intelligent Vehicles. This is the author's version which has not been fully edited and content may change prior to final publication. Citation information: DOI 10.1109/TIV.2024.3404658

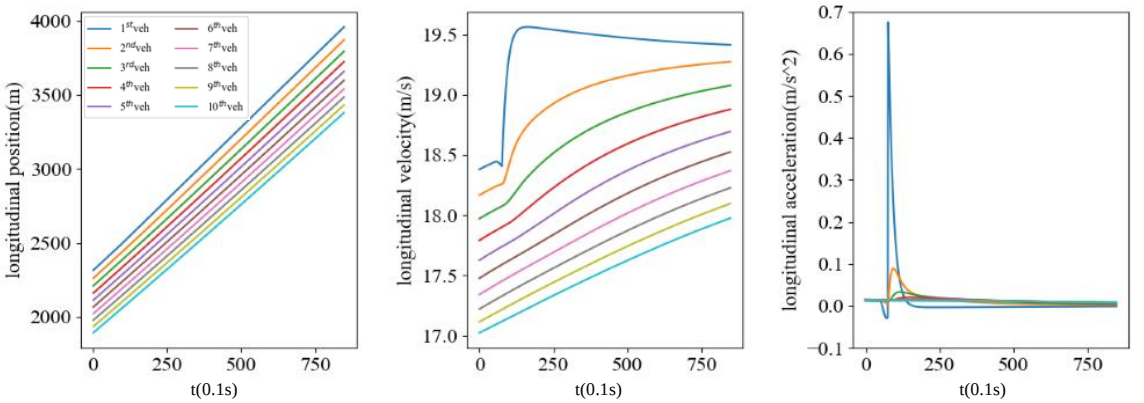

(a) rear vehicle trajectories in the current lane with the general algorithm

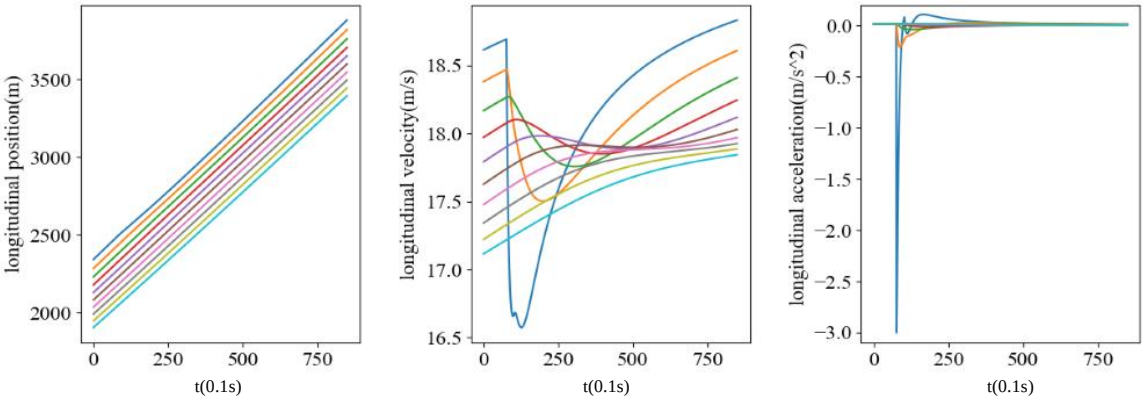

(b) rear vehicle trajectories in the target lane with the general algorithm

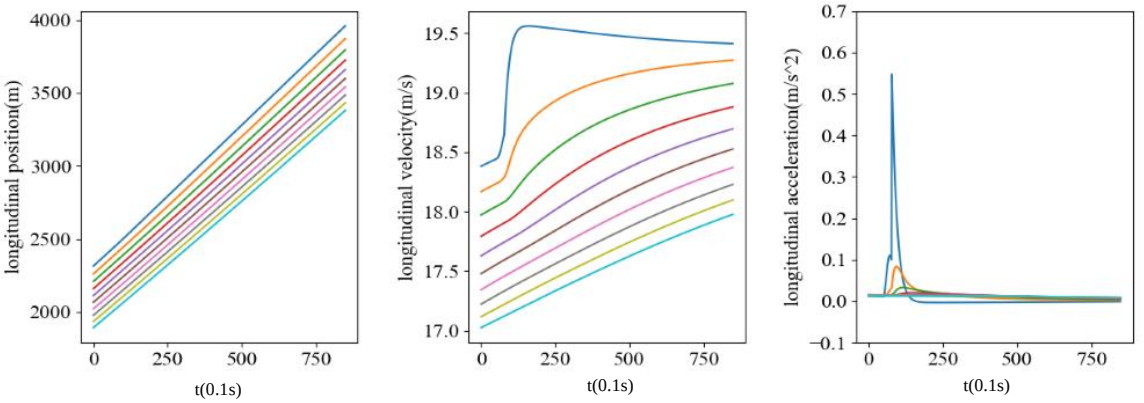

(c) rear vehicle trajectories in the current lane with our algorithm

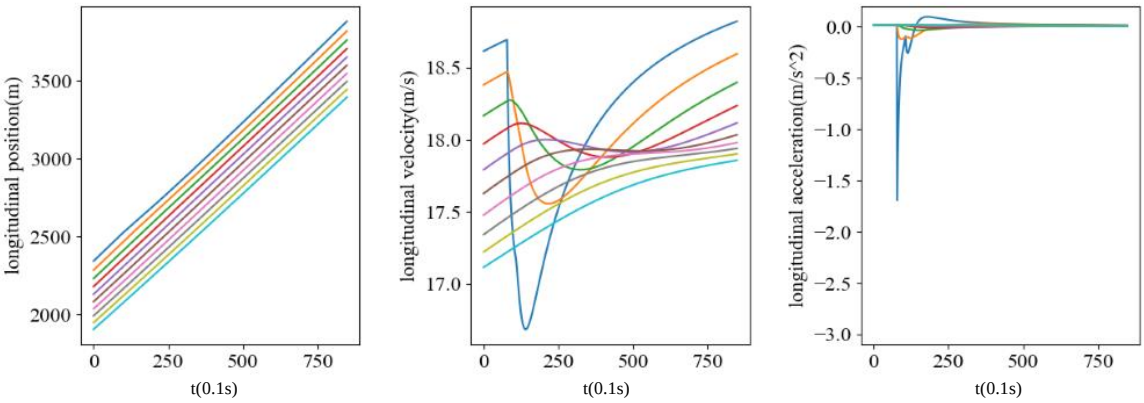

(d) rear vehicle trajectories in the target lane with our algorithm

Fig. 11. Trajectories of 10 rear vehicles of SV with an initial flow speed at 15m/s

This article has been accepted for publication in IEEE Transactions on Intelligent Vehicles. This is the author's version which has not been fully edited and content may change prior to final publication. Citation information: DOI 10.1109/TIV.2024.3404658

Table 8. Performance of rear vehicles with an initial flow speed at 15m/s

Vehicle ID	General algorithm		Our algorithm		Baseline algorithm		Local optimum algorithm	
	Current lane	Target lane	Current lane	Target lane	Current lane	Target lane	Current lane	Target lane
150-metre travel time (s)								
FV1	8.1	8.7	7.9	8.4	8.1	8.5	7.9	8.2
FV2	8.3	8.3	8.2	8.2	8.3	8.3	8.1	8.2
FV3	8.4	8.3	8.3	8.3	8.4	8.3	8.2	8.3
FV4	8.4	8.3	8.4	8.3	8.4	8.3	8.4	8.3
FV5	8.5	8.4	8.5	8.4	8.5	8.4	8.5	8.4
FV6	8.6	8.5	8.6	8.5	8.6	8.5	8.6	8.5
FV7	8.6	8.6	8.6	8.6	8.6	8.6	8.6	8.6
FV8	8.7	8.6	8.7	8.6	8.7	8.6	8.7	8.6
FV9	8.8	8.7	8.8	8.7	8.8	8.7	8.8	8.7
FV10	8.8	8.8	8.8	8.8	8.8	8.8	8.8	8.8
15-second travel distance (m)								
FV1	286.7	257.7	289.0	262.5	286.8	259.9	291.1	267.2
FV2	276.2	268.6	278.4	272.3	276.3	269.9	280.6	273.8
FV3	271.1	271.7	273.2	273.5	271.2	272.3	275.3	273.8
FV4	269.8	271.1	269.8	271.4	269.8	271.3	269.9	271.8
FV5	267.2	269.2	267.2	269.3	267.2	269.3	267.2	269.4
FV6	264.9	267.0	264.9	267.0	264.9	267.0	264.9	267.1
FV7	262.8	264.8	262.8	264.8	262.8	264.8	262.8	264.9
FV8	260.9	262.8	260.9	262.8	260.9	262.8	260.9	262.8
FV9	259.2	260.9	259.2	260.9	259.2	260.9	259.2	260.9
FV10	257.7	259.2	257.7	259.2	257.7	259.2	257.7	259.2
Total	2676.5	2653.0	2683.1	2663.7	2676.8	2657.4	2689.6	2670.9
Maximum acceleration/deceleration during lane change (m/s^2)								
FV1	0.67	3.00	0.54	1.68	0.59	2.18	0.33	0.37
FV2	0.09	0.21	0.08	0.13	0.09	0.16	0.07	0.05
FV3	0.04	0.04	0.03	0.02	0.03	0.03	0.03	0.01
FV4	0.02	-	0.02	-	0.02	-	0.02	-
FV5	0.02	-	0.02	-	0.02	-	0.02	-
FV6	0.02	-	0.02	-	0.02	-	0.02	-
FV7	0.02	-	0.02	-	0.02	-	0.02	-
FV8	0.02	-	0.02	-	0.02	-	0.02	-
FV9	0.02	-	0.02	-	0.02	-	0.02	-
FV10	0.02	-	0.02	-	0.02	-	0.02	-
Speed increase/decrease rate during lane change								
FV1	4.91%	10.81%	5.38%	7.99%	5.18%	9.02%	5.89%	4.09%
FV2	1.14%	2.35%	1.53%	1.53%	1.31%	1.93%	2.12%	0.56%
FV3	0.48%	0.20%	0.65%	0.08%	0.59%	0.15%	0.98%	0.11%
FV4	0.43%	-	0.52%	-	0.47%	-	0.69%	-
FV5	0.43%	-	0.51%	-	0.47%	-	0.63%	-
FV6	0.42%	-	0.49%	-	0.47%	-	0.62%	-
FV7	0.42%	-	0.48%	-	0.47%	-	0.62%	-
FV8	0.42%	-	0.48%	-	0.47%	-	0.61%	-
FV9	0.40%	-	0.47%	-	0.48%	-	0.59%	-
FV10	0.38%	-	0.44%	-	0.42%	-	0.56%	-

Note: "-" in the table represents the value not available (i.e., no deceleration or speed decrease rate is observed).

This article has been accepted for publication in IEEE Transactions on Intelligent Vehicles. This is the author's version which has not been fully edited and content may change prior to final publication. Citation information: DOI 10.1109/TIV.2024.3404658

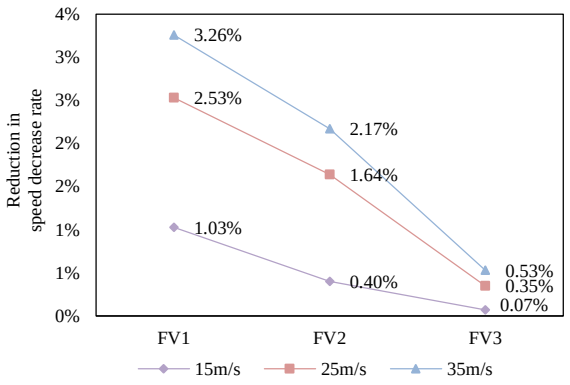

Fig. 12. Lane-changing efficiency improvement in the target lane with different initial flow speeds

C2. Lane change safety

To verify the safety performance of the proposed improved potential field, based on a real trajectory extracted from Zen Traffic Data, a new lane-changing trajectory was planned using the proposed algorithm and was compared with the real trajectory in terms of collision risk. In the study, the inverse of Time-to-Collision (TTC) between SV and its four neighboring vehicles during lane change was calculated to quantify the trajectory risk. The inverse of TTC (1/TTC) is a commonly used indicator of vehicle driving safety, and the higher the value, the greater the likelihood of a conflict between the two vehicles. Fig. 13 shows the box plots of the calculated 1/TTC, where the blue ones correspond to the lane-changing trajectory planned based on the proposed predicted risk field, and the red ones represent the safety performance under the real trajectory. Compared with our algorithm, the 1/TTC between SV and neighboring vehicles under the real trajectory is generally higher, especially for SV and its rear vehicle in the current lane. This indicates that the proposed predictive risk field can effectively describe the interaction risk of SV during lane changing, based on which safer lane-changing trajectories can be planned using our proposed framework.

An ordinary potential field method, which does not account for the uncertainty in acceleration and direction (as described in [20]), was further used to plan new lane-changing trajectories based on the real trajectories in comparison with the proposed method. Two composite lane-changing risk indicators, i.e., the Lane-Changing Risk Index (LCRI) [43] and the Lane-changing Adjacent-vehicle Risk (LAR) [44], were employed to assess the risk of the planned lane-changing trajectories. LCRI quantifies the probability and severity of collisions in lane changing, and LAR combines the maximum lateral and longitudinal risks during the lane-changing process. Both LCRI and LAR range from 0 to 1, and the higher the values of these indicators, the higher the risk of the planned lane-changing trajectories. Furthermore, in order to assess the safety performance of the two potential field methods in different speed scenarios, the real lane-changing trajectories were divided into three equal-sized groups according to the speed of SV at the start of lane change, i.e., the low speed (0~33rd percentile speed), medium speed (33~66th percentile speed), and high speed (66~100th percentile speed) groups. Fig. 14 shows that while the risk indicator values of the two methods are close in the low speed group, the proposed method exhibits a lower risk profile than the ordinary method in the medium and high speed groups. In other words, the proposed potential field method has a better performance in producing safer lane-changing trajectories, especially in higher-speed scenarios.

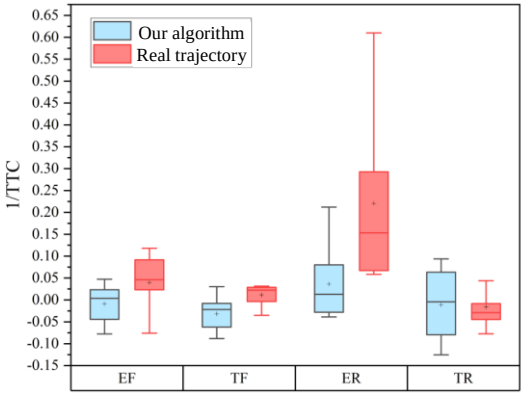

Note: EF = Ego-lane front vehicle; TF = Target-lane front vehicle; ER = Ego-lane rear vehicle; TR = Target-lane rear vehicle.

Fig. 13. Longitudinal risks in the lane changing process

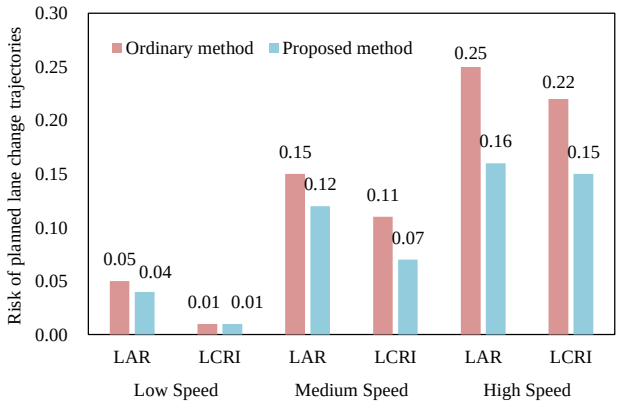

Fig. 14. Lane-changing risk using the proposed vs. ordinary potential field methods

VI. Conclusion

The paper proposed a CAV lane-changing trajectory planning method that simultaneously considers the benefits of SV, the rear vehicles in the current lane, and the rear vehicles in the target lane, which achieves a beneficial impact on the traffic flow while satisfying safe and efficient lane-changing for SV. In particular, a novel evaluation scheme and an ordered probit model were proposed to assess and predict the number of affected rear vehicles in the current and target lanes. The benefits of the affected rear vehicles were then incorporated into the cost function to improve the effectiveness of the lane-changing algorithm. An improved potential field was also developed to better characterize the safety situation of the planned trajectories. The SUMO simulation results showed that the proposed algorithm can generate lane-changing trajectories with less impact on the rear traffic while maintaining the benefits of SV compared with other algorithms. The planned lane-changing trajectories

also showed generally higher safety performance in comparison with those planned by an ordinary potential field method. The results of this paper highlight the importance of considering the benefits of the surrounding vehicles under the influence of lane changes, and can provide a reference for trajectory planning of CAVs in multi-vehicle interaction scenarios.

In this paper, the classical IDM model has been used to describe the car-following behavior of the rear vehicles during lane changes in the cost function. However, whether there is a better car-following model that can provide more accurate cost estimates still needs to be further investigated. Also, more accurate learning-based algorithms can be investigated in the future to quantify the number of affected rear vehicles given more diversified trajectory data [45]-[47]. In addition, how to integrate lane-change decision-making with trajectory planning considering their impact on surrounding vehicles is an important issue to be addressed in the next phase. Looking to the future, as large-scale models such as ChatGPT have shown great potential in the field of transportation [48],[49], the adaptability and learning capability of the large models should be further explored to develop more comprehensive trajectory planning schemes for CAVs in complex traffic scenarios [50].

ACKNOWLEDGMENT

The authors thank Hanshin Expressway Company for providing the Zen Traffic Data.

REFERENCES

[1] NHTSA, "Traffic Safety Facts 2020: A Compilation of Motor Vehicle Crash Data," National Highway Traffic Safety Administration, Washington, DC, USA, Oct. 2022.

[2] L. Li, J. Gan, K. Zhou, X. Qu, and B. Ran, "A novel lane-changing model of connected and automated vehicles: Using the safety potential field theory," *Phys. A Stat. Mech. its Appl.*, vol. 559, p. 125039, 2020, doi: 10.1016/j.physa.2020.125039.

[3] M. Wang, S. Hoogendoorn, W. Daamen, B. van Arem, and R. Happee, "Game theoretic approach for predictive lane-changing and car-following control," *Transp. Res. Part C Emerg. Technol.*, vol. 58, pp. 73–92, 2015, doi: 10.1016/j.trc.2015.07.009.

[4] Y. Wang, L. Wang, J. Guo, I. Papamichail, M. Papageorgiou, and F. Wang, et al., "Ego-efficient lane changes of connected and automated vehicles with impacts on traffic flow," *Transp. Res. Part C Emerg. Technol.*, vol. 138, p. 103478, 2022, doi: 10.1016/j.trc.2021.103478.

[5] X. Liu, N. Masoud, Q. Zhu, and A. Khojandi, "A Markov Decision Process framework to incorporate network-level data in motion planning for connected and automated vehicles," *Transp. Res. Part C Emerg. Technol.*, vol. 136, no. January, p. 103550, 2022, doi: 10.1016/j.trc.2021.103550.

[6] Y. Li, L. Li, D. Ni, and W. Wang, "Automatic Lane-Changing Trajectory Planning:From Self-optimum to Local-optimum," *IEEE Trans. Intell. Transp. Syst.*, vol. 23, no. 11, pp. 21004-21014, 2022, doi: 10.1109/TITS.2022.3179117.

[7] T. Pan, W. Lam, A. Sumalee, and R. Zhong, "Modeling the impacts of mandatory and discretionary lane-changing maneuvers," *Transp. Res. Part C Emerg. Technol.*, vol. 68, pp. 403–424, 2016, doi: 10.1016/j.trc.2016.05.002.

[8] X. Li and J. Q. Sun, "Studies of vehicle lane-changing dynamics and its effect on traffic efficiency, safety and environmental impact," *Phys. A Stat. Mech. its Appl.*, vol. 467, pp. 41–58, 2017, doi: 10.1016/j.physa.2016.09.022.

[9] Z. Zheng, S. Ahn, D. Chen, and J. Laval, "Freeway traffic oscillations: Microscopic analysis of formations and propagations using Wavelet Transform," *Procedia - Soc. Behav. Sci.*, vol. 17, pp. 702–716, 2011, doi: 10.1016/j.sbspro.2011.04.540.

[10] M. Li, Z. Li, C. Xu, and T. Liu, "Short-term prediction of safety and operation impacts of lane changes in oscillations with empirical vehicle trajectories," *Accid. Anal. Prev.*, vol. 135, p. 105345, 2020, doi: 10.1016/j.aap.2019.105345.

[11] J. He, J. Qu, J. Zhang, and Z. He, "The Impact of a Single Discretionary Lane Change on Surrounding Traffic: An Analytic Investigation," *IEEE Trans. Intell. Transp. Syst.*, vol. 24, no. 1, pp. 554–563, 2023, doi: 10.1109/TITS.2022.3209668.

[12] Q. Yang, F. Lu, J. Ma, X. Niu, and J. Wang, "Analyzing the delays of target lane vehicles caused by vehicle lane-changing operation," *Sci. Rep.*, vol. 11, no. 1, pp. 1–10, 2021, doi: 10.1038/s41598-021-00262-1.

[13] Q. Chen, H. Huang, Y. Li, J. Lee, K. Long, R. Gu, and X. Zhai, "Modeling accident risks in different lane-changing behavioral patterns," *Anal. Methods Accid. Res.*, vol. 30, p. 1001592021, doi: 10.1016/j.amar.2021.100159.

[14] X. Liu, J. Liang, and H. Zhang, "Dynamic motion planner with trajectory optimisation for automated highway lanechanging driving," *IET Intell. Transp. Syst.*, vol. 14, no. 14, pp. 2133–2140, 2020, doi: 10.1049/iet-its.2020.0465.

[15] Y. Luo, Y. Xiang, K. Cao, and K. Li, "A dynamic automated lane change maneuver based on vehicle-to-vehicle communication," *Transp. Res. Part C Emerg. Technol.*, vol. 62, pp. 87–102, 2016, doi: 10.1016/j.trc.2015.11.011.

[16] F. Garrido and P. Resende, "Review of Decision-Making and Planning Approaches in Automated Driving," *IEEE Access*, vol. 10, no. 8, pp. 100348–100366, 2022, doi: 10.1109/ACCESS.2022.3207759.

[17] A. Pierson, W. Schwarting, S. Karaman, and D. Rus, "Learning risk level set parameters from data sets for safer driving," *IEEE Intell. Veh. Symp. Proc.*, vol. 2019, no. 4, pp. 273–280, 2019, doi: 10.1109/IVS.2019.8813842.

[18] J. Wu, X. Chen, Y. Bie, and W. Zhou, "A co-evolutionary lane-changing trajectory planning method for automated vehicles based on the instantaneous risk identification," *Accid. Anal. Prev.*, vol. 180, p. 106907, 2023, doi: 10.1016/j.aap.2022.106907.

[19] C. Cai, C. Teng, X. Xiong, H. Wang, X. Sun, and Q. Liu, "Complex environment model, cognitive system and cognitive method of autonomous vehicle based on complex network," JP Patent 2022-553145, Mar. 12, 2024.

[20] K. Lee and D. Kum, "Collision avoidance/mitigation system: Motion planning of autonomous vehicle via predictive occupancy map," *IEEE Access*, vol. 7, pp. 52846–52857, 2019, doi: 10.1109/ACCESS.2019.2912067.

[21] B. Paden, M. Čáp, S. Z. Yong, D. Yershov, and E. Frazzoli, "A survey of motion planning and control techniques for self-driving urban vehicles," *IEEE Trans. Intell. Veh.*, vol. 1, no. 1, pp. 33–55, 2016, doi: 10.1109/TIV.2016.2578706.

[22] T. Stahl, A. Wischnewski, J. Betz, and M. Lienkamp, "Multilayer Graph-Based Trajectory Planning for Race Vehicles in Dynamic Scenarios," *2019 IEEE Intell. Transp. Syst. Conf. ITSC 2019*, pp. 3149–3154, 2019, doi: 10.1109/ITSC.2019.8917032.

[23] G. Tanzmeister, D. Wollherr, and M. Buss, "Grid-Based Multi-Road-Course Estimation Using Motion Planning," *IEEE Trans. Veh. Technol.*, vol. 65, no. 4, pp. 1924–1935, 2016, doi: 10.1109/TVT.2015.2420752.

[24] T. Guy, J. M. Dolan, and J. W. Lee, "Automated tactical maneuver discovery, reasoning and trajectory planning for autonomous driving," *IEEE Int. Conf. Intell. Robot. Syst.*, vol. 2016, pp. 5474–5480, 2016, doi: 10.1109/IROS.2016.7759805.

[25] D. Shen, Y. Chen, L. Li, and S. Chien, "Collision-Free Path Planning for Automated Vehicles Risk Assessment via Predictive Occupancy Map," *IEEE Intell. Veh. Symp. Proc.*, no. 4, pp. 985–991, 2020, doi: 10.1109/IV47402.2020.9304720.

[26] S. Yang, H. Zheng, J. Wang, and A. El Kamel, "A Personalized Human-Like Lane-Changing Trajectory Planning Method for Automated Driving System," *IEEE Trans. Veh. Technol.*, vol. 70, no. 7, pp. 6399–6414, 2021, doi: 10.1109/TVT.2021.3083268.

[27] L. Chen, D. Qin, X. Xu, Y. Cai, and J. Xie, "A path and velocity planning method for lane changing collision avoidance of intelligent vehicle based on cubic 3-D Bezier curve," *Adv. Eng. Softw.*, vol. 132, pp. 65–73, 2019, doi: 10.1016/j.advengsoft.2019.03.007.

[28] Z. Zhang, C. Wang, W. Zhao, M. Cao, J. Liu, and K. Xu, "Path-speed decoupling planning method based on risk cooperative game for

intelligent vehicles," *IEEE Trans. Transp. Electrif.*, vol. PP, p. 1, 2023, doi: 10.1109/TTE.2023.3316124.
[29] W. Lim, S. Lee, M. Sunwoo, and K. Jo, "Hybrid Trajectory Planning for Autonomous Driving in On-Road Dynamic Scenarios," *IEEE Trans. Intell. Transp. Syst.*, vol. 22, no. 1, pp. 341–355, 2021, doi: 10.1109/TITS.2019.2957797.
[30] Y. Ji, L. Ni, C. Zhao, C. Lei, Y. Du, and W. Wang, "TriPField: A 3D Potential Field Model and Its Applications to Local Path Planning of Autonomous Vehicles," *IEEE Trans. Intell. Transp. Syst.*, vol. 24, no. 3, pp. 3541–3554, 2023, doi: 10.1109/TITS.2022.3231259.
[31] S. Xie, J. Hu, P. Bhowmick, Z. Ding, and F. Arvin, "Distributed Motion Planning for Safe Autonomous Vehicle Overtaking via Artificial Potential Field," *IEEE Trans. Intell. Transp. Syst.*, vol. 23, no. 11, pp. 21531–21547, 2022, doi: 10.1109/TITS.2022.3189741.
[32] Y. Shang, F. Zhu, R. Jiang, X. Li, and S. Wang, "Trajectory planning at a signalized road section in a mixed traffic environment considering lane-changing of CAVs and stochasticity of HDVs," *Transp. Res. Part C Emerg. Technol.*, vol. 158, p. 104441, 2024, doi: 10.1016/j.trc.2023.104441.
[33] Q. Dong, Z. Yan, K. Nakano, X. Ji, and Y. Liu, "Graph-Based Scenario-Adaptive Lane-Changing Trajectory Planning for Autonomous Driving," *IEEE Robot. Autom. Lett.*, vol. 8, no. 9, pp. 5688–5695, 2023, doi: 10.1109/LRA.2023.3300250.
[34] Z. Yao, H. Deng, Y. Wu, B. Zhao, G. Li, and Y. Jiang, "Optimal lane-changing trajectory planning for autonomous vehicles considering energy consumption," *Expert Syst. Appl.*, vol. 225, p. 120133, 2023, doi: 10.1016/j.eswa.2023.120133.
[35] C. Yang, X. Chen, X. Lin, and M. Li, "Coordinated trajectory planning for lane-changing in the weaving areas of dedicated lanes for connected and automated vehicles," *Transp. Res. Part C Emerg. Technol.*, vol. 144, p. 103864, 2022, doi: 10.1016/j.trc.2022.103864.
[36] Y. Li, L. Li, and D. Ni, "Dynamic Trajectory Planning for Automated Lane Changing Using the Quintic Polynomial Curve," *J. Adv. Transp.*, vol. 2023, p. 6926304, doi: 10.1155/2023/6926304.
[37] C. Huang *et al.*, "Personalized Trajectory Planning and Control of Lane-Change Maneuvers for Autonomous Driving," *IEEE Trans. Veh. Technol.*, vol. 70, no. 6, pp. 5511–5523, 2021, doi: 10.1109/TVT.2021.3076473.
[38] D. Xiao, Ž. Šarić, X. Xu, and Q. Yuan, "Investigating injury severity of pedestrian–vehicle crashes by integrating latent class cluster analysis and unbalanced panel mixed ordered probit model," *J. Transp. Saf. Secur.*, vol. 15, no. 2, pp. 83–102, 2023, doi: 10.1080/19439962.2022.2033900.
[39] P. G. Gipps, "A model for the structure of lane-changing decisions," *Transp. Res. Part B*, vol. 20, no. 5, pp. 403–414, 1986, doi: 10.1016/0191-2615(86)90012-3.
[40] The Hanshin Expressway Company, "Zen Traffic Data, " Project ZTD, https://zen-traffic-data.net, 2018 (accessed Feb. 2023).
[41] Y. Chen, R. Yuan, J. Wei, and S. Li, "Research on the influencing factors of elderly pedestrian traffic accidents considering the built environment," *Int. Rev. Spat. Plan. Sustain. Dev.*, vol. 11, no. 1, pp. 44–63, 2023, doi: 10.14246/irspsd.11.1_44.
[42] Y. Zhang, Q. Xu, J. Wang, K. Wu, Z. Zheng, and K. Lu, "A Learning-Based Discretionary Lane-Change Decision-Making Model With Driving Style Awareness," *IEEE Trans. Intell. Transp. Syst.*, vol. 24, no. 1, pp. 68–78, 2023, doi: 10.1109/TITS.2022.3217673.
[43] H. Park, C. Oh, J. Moon, and S. Kim, "Development of a lane change risk index using vehicle trajectory data," *Accid. Anal. Prev.*, vol. 110, pp. 1–8, 2018, doi: 10.1016/j.aap.2017.10.015.
[44] X. Xiong, Y. He, Y. Cai, Q. Liu, H. Wang, and L. Chen, "Multi-Level Prediction Framework of Driving Risk Based on the Matter-Element Extension Model," *Transp. Res. Rec. J. Transp. Res. Board*, vol. 0(0), Jan. 2024, doi: 10.1177/03611981231223750.
[45] Y. Fei, P. Shi, Y. Li, Y. Liu, X. Qu, "Formation control of multi-agent systems with actuator saturation via neural-based sliding mode estimators, " *Knowl. Based Syst.*, vol. 284, p. 111292, 2024, doi: 10.1016/j.knosys.2023.111292.
[46] Y. He, Y. Liu, L. Yang and X. Qu, "Deep Adaptive Control: Deep Reinforcement Learning-Based Adaptive Vehicle Trajectory Control Algorithms for Different Risk Levels," *IEEE Trans. Intell. Veh*, vol. 9, no. 1, pp. 1654-1666, 2024, doi: 10.1109/TIV.2023.3303408.
[47] Y. Liu, R. Jia, J. Ye, X. Qu, "How machine learning informs ride-hailing services: A survey, " *Commun. Transport. Res.*, vol. 2, p. 1000752022, 2022, doi: 10.1016/j.commtr.2022.100075.
[48] X. Qu, H. Lin, and Y. Liu, "Envisioning the future of transportation: Inspiration of ChatGPT and large models," *Commun. Transp. Res.*, vol. 3, p. 100103, 2023, doi: 10.1016/j.commtr.2023.100103.
[49] Y. Liu, F. Wu, Z. Liu, K. Wang, F. Wang, and X. Qu, "Can language models be used for real-world urban-delivery route optimization?," *Innovation*, vol. 4, no. 6, p. 100520, 2023, doi: 10.1016/j.xinn.2023.100520.
[50] F. Y.Wang and C. Lv, "Foundation vehicles: From foundation intelligence to foundation transportation for future mobility," *IEEE Trans. Intell. Veh.*, vol. 8, no. 10, pp. 4287-4291, 2023, doi 10.1109/TIV.2023.3326636

Xiaoxia Xiong received a B.S. degree in transportation engineering from Southeast University, Jiangsu, China, in 2009, an M.S. degree in civil engineering from the University of Texas at Austin, Texas, the U.S., in 2012, and a Ph.D. degree in transportation engineering from Jiangsu University, China. She is currently a lecturer at the School of Automotive and Traffic Engineering of Jiangsu University, China. Her research interests include road traffic safety and management, vehicle active safety technology, and machine learning and data mining.

Yu He received a B.S. degree in transportation engineering from Northeast Forestry University, Heilongjiang, China, in 2021. He is currently pursuing his M.S. degree at Jiangsu University. His research interests include road traffic safety and autonomous vehicles.

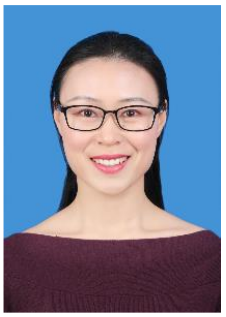

Yingfeng Cai (M'17-SM'21) received B.S., M.S., and Ph.D. degrees from the School of Instrument Science and Engineering, Southeast University, Nanjing, China, respectively. In 2013, she joined the Automotive Engineering Research Institute at Jiangsu University, where now, she is working as a professor. Her research interests include computer vision, intelligent transportation systems, and intelligent automobiles.

Qingchao Liu received a Ph.D. degree in transportation engineering from Southeast University, Jiangsu, China, in 2015. He is currently an associate professor at Jiangsu University. His research interests include intelligent decision-making and coordinated control of connected autonomous vehicles.

Hai Wang (M'17-SM'21) received B.S., M.S., and Ph.D. degrees from the School of Instrument Science and Engineering, Southeast University, Nanjing, China, respectively. In 2012, he joined the School of Automotive and Traffic Engineering at Jiangsu University, where now, he is working as a professor. His research interests include computer vision, intelligent transportation systems, and intelligent vehicles. He has published more than 50 papers in the field of machine vision-based environment sensing for intelligent vehicles.

Long Chen received his Ph.D. degree in Vehicle Engineering from Jiangsu University, Zhenjiang, China, in 2002. His research interests include intelligent automobiles and vehicle control systems.